

Time-Delay-Domain and Pseudorandom-Noise Photoacoustic and Photothermal Wave Processes: A Review of the State of the Art

ANDREAS MANDELIS

Abstract—The application and development of correlation and spectral analysis methods to photoacoustic and photothermal wave detection are examined. The purposes of this review are to 1) describe the two most prominent techniques available for photothermal correlation and spectral processing, namely the pseudorandom noise and the frequency-modulation (FM) time-delay (or frequency sweep) optical excitation; 2) compare the technical features of these techniques, such as measurement dynamic range properties, amount of measurement time required and instrumentation requirements; and 3) present advantages of the techniques over the widely used conventional frequency domain and pulsed laser excitation, as well as a detailed comparison between themselves. Attention is focused on the conceptual and mathematical details of signal generation, processing, and interpretation. Subtle but significant differences in the signal dynamic range, impulse response, and transfer function are shown to determine the limits of each of the two major techniques and are corroborated by the available experimental evidence to date. A review of the steadily increasing literature on spectroscopic and thermal imaging applications of these techniques is a powerful indicator of the promise they hold for conducting fundamental and applied studies, primarily due to 1) the superior wealth of information obtained through pseudorandom photothermal excitation, as compared to the conventional frequency dispersive techniques and 2) the less destructive nature of the pseudorandom impulse response, compared to pulsed laser excitation.

I. BACKGROUND

A. Nature of Random Signals and Classification of Correlation and Spectral Functions

RANDOM SIGNALS and random physical phenomena, in general, cannot be described explicitly in terms of mathematical functions, because, by the very definition of randomness, there is no apparent physical law that governs the physical response of a given system. Another frequently used term to denote the same physical response of a system acted upon by some chance mechanism is "stochastic signal." Even though no single mathematical description of such a system response exists, the response can be described, however, by averaging values over a large set of sample functions (an ensemble) taken at specific times and forming the time history of the ran-

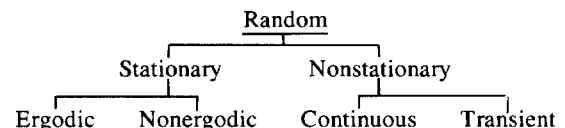
dom response of the system. If the symbol $\{ \}$ is used to denote such an ensemble of sample functions, two primitive mathematical functions can be defined as statistical descriptions of the random process, namely [1] a mean value

$$\mu_x(t_1) = \lim_{N \rightarrow \infty} \frac{1}{N} \sum_{k=1}^N X_k(t_1) \quad (1.1)$$

and an autocorrelation function

$$R_{xx}(t_1, t_1 + \tau) = \lim_{N \rightarrow \infty} \frac{1}{N} \sum_{k=1}^N X_k(t_1) X_k(t_1 + \tau) \quad (1.2)$$

where the summations are taken over the ensemble $\{X(t)\}$. The autocorrelation function is a measure of the degree of correlation between the values of the random signal at two different times t_1 and $t_1 + \tau$. The following shows all the possible classifications of random signals:



Of greatest importance to photoacoustic and photothermal wave spectroscopies are the signals of stationary nature. These are random signals characterized by (1.1) and (1.2), in the special event that μ_x and R_{xx} do not vary with time. Thus these two functions are independent of the particular sample record used to determine them:

$$\mu_x(t_1) = \mu_x = \text{constant} \quad (1.3)$$

and

$$R_{xx}(t_1 + \tau) = R_{xx}(\tau). \quad (1.4)$$

According to the ergodic hypothesis for a random stationary process, the observation of N arbitrarily chosen sample functions from the ensemble $\{X(t)\}$ is statistically equivalent to a large number of observations made on a single sample function at N arbitrary instants of time. For closely spaced observation instants of time of the k th sample function, the mean value $\mu_x(k)$ and the autocorrelation function $R_{xx}(\tau, k)$ are given by

Manuscript received December 8, 1985; revised February 6, 1986.

The author is with the Photoacoustic and Photothermal Sciences Laboratory, Department of Mechanical Engineering, University of Toronto, Toronto, ON M5S 1A4, Canada.

IEEE Log Number 8609271.

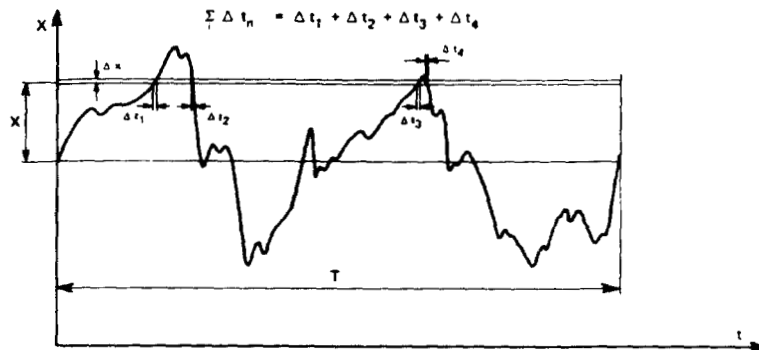


Fig. 1. Illustration of probability density for a stationary random signal [3].

$$\mu_x(k) = \lim_{T \rightarrow \infty} \frac{1}{T} \int_0^T X_k(t) dt = \mu_x \quad (1.5)$$

and

$$R_{xx}(\tau, k) = \lim_{T \rightarrow \infty} \frac{1}{T} \int_0^T X_k(t) X_k(t + \tau) dt = R_{xx}(\tau). \quad (1.6)$$

Only stationary random signals can be ergodic [2], which is responsible for their exclusive role in photoacoustics. Nonstationary signals can be broadly divided into continuous nonstationary, i.e., signals with no beginning or end, and transient nonstationary signals that start and finish at zero. In practice, short segments of continuous signals are used for analysis, called quasi-stationary. The stochastic nature of stationary random signals allows only a probabilistic interpretation, as illustrated in Fig. 1. It is clear from this figure that the probability density $p(X)$ that the signal value lies between X and $X + \Delta X$ is given by

$$p(X) = \lim_{\Delta X \rightarrow 0} \left[\frac{P(X + \Delta X) - P(X)}{\Delta X} \right] \quad (1.7)$$

where $P(X)$ represents the total probability that the signal value is less than X . Furthermore, Fig. 1 shows that

$$P(X + \Delta X) - P(X) = \lim_{T \rightarrow \infty} \left[\frac{\sum \Delta t_n}{T} \right] \quad (1.8)$$

where each Δt_n represents one of the time intervals in T , where the signal lies between X and $X + \Delta X$. It can be shown [4] that the probability density function for a stationary random process (noise) has a Gaussian shape of the form

$$p(X) = \frac{1}{\sigma\sqrt{2\pi}} \exp \left[-\frac{1}{2} \frac{(X - \mu_x)^2}{\sigma^2} \right] \quad (1.9)$$

where σ denotes the standard deviation from the mean value μ_x .

The assumed ergodicity of stationary random signals allows the elimination of the subscript k from the sample function $X_k(t)$ in (1.5) and (1.6), a convenient simplification for experimental systems, which record such signals within one finite observation time interval T . There-

fore, for experimental photoacoustic and photothermal wave situations, (1.5) and (1.6) become

$$\mu_x = \lim_{T \rightarrow \infty} \frac{1}{T} \int_0^T X(t) dt, \quad [V] \quad (1.10)$$

and

$$R_{xx}(\tau) = \lim_{T \rightarrow \infty} \frac{1}{T} \int_0^T X(t) X(t + \tau) dt, \quad [V^2]. \quad (1.11)$$

The autocorrelation function $R_{xx}(\tau)$ in (1.11) provides a measure of the similarity between the input signal $X(t)$ and its own time-delayed version $X(t + \tau)$. As the input random signal to a photothermal system results in a random output signal [5], it is necessary to introduce statistical functions that measure the degree of correlation between input and output signals. The statistical correlation functions of importance to random photothermal wave signal analysis, besides the autocorrelation function and the mean, are 1) the cross-correlation and unit impulse response functions in the time domain and 2) the one-sided autospectral and cross-spectral densities, the coherence function, coherent output power spectrum and transfer function in the frequency domain [6]. A brief synopsis of these functions in terms of definitions and significance is as follows: The cross-correlation function between the system input stationary random signal/sample function $X(t)$, and the output signal $Y(t)$ is given by

$$R_{xy}(\tau) = \lim_{T \rightarrow \infty} \frac{1}{T} \int_0^T X(t) Y(t + \tau) dt \quad [V^2]. \quad (1.12)$$

This function provides a measure of the similarity between the input signal $X(t)$ and a time-delayed version of the output signal $Y(t + \tau)$. In the frequency domain the input one-sided autospectral density is an experimentally meaningful function

$$G_{xx}(f) = 4 \int_0^\infty R_{xx}(\tau) \cos(2\pi f\tau) dt \quad [V^2/Hz] \quad (1.13)$$

which measures the rate of change of the average input signal power with frequency. An entirely analogous definition can be given for the output one-sided autospectral density $G_{yy}(f)$. The one-sided cross-spectral density

$$g_{xy}(f) = 4 \int_0^{\infty} R_{xy}(\tau) \cos(2\pi f\tau) d\tau \quad [\text{V}^2/\text{Hz}] \quad (1.14)$$

is a measure of the frequency interrelationship between the random input signal $X(t)$ and the time-delayed version of the output signal $Y(t + \tau)$. Unlike the autocorrelation function, the cross-correlation function $R_{xy}(\tau)$ is not an even function of the delay time. For this reason additional information about a photothermal wave system can be obtained by extending the cosine Fourier transform of (1.14) to include all times, which defines the cross-spectrum

$$\begin{aligned} G_{xy}(f) &= 2 \int_{-\infty}^{\infty} R_{xy}(\tau) e^{-2i\pi f\tau} d\tau \\ &\equiv C_{xy}(f) - iQ_{xy}(f). \end{aligned} \quad (1.15)$$

The real part

$$C_{xy}(f) = 2 \int_{-\infty}^{\infty} R_{xy}(\tau) \cos(2\pi f\tau) d\tau \quad (1.16)$$

is called the cospectrum, while the imaginary part

$$Q_{xy}(f) = 2 \int_{-\infty}^{\infty} R_{xy}(\tau) \sin(2\pi f\tau) d\tau \quad (1.17)$$

is called the quadspectrum. In polar coordinate notation the magnitude and phase of the cross-spectrum are given by

$$|G_{xy}(f)| = [C_{xy}^2(f) + Q_{xy}^2(f)]^{1/2} \quad [\text{V}^2/\text{Hz}] \quad (1.18)$$

and

$$\theta_{xy}(f) = \tan^{-1} \left[\frac{Q_{xy}(f)}{C_{xy}(f)} \right] \quad [\text{rad}]. \quad (1.19)$$

Physically, the cross-spectral magnitude is a measure of the frequency content of the causal response of a system induced by a random input $X(t)$, while the phase carries information about the propagation time between input and output. This time delay manifests itself as a linear phase shift. The coherence function is defined as

$$\begin{aligned} \gamma_{xy}^2(f) &= \frac{|G_{xy}(f)|^2}{G_{xx}(f) G_{yy}(f)}, \\ 0 &\leq \gamma_{xy}^2(f) \leq 1 \quad (\text{dimensionless}). \end{aligned} \quad (1.20)$$

This function constitutes a powerful indicator of the strength of the relation between the input signal and output response of a randomly excited photoacoustic/photothermal system. A very useful related function is the coherent output power spectrum

$$\gamma_{xy}^2(f) G_{yy}(f) = \frac{|G_{xy}(f)|^2}{G_{xx}(f)} \quad [\text{V}^2/\text{Hz}]. \quad (1.21)$$

This function is a measure of the output power spectrum caused by the input excitation in the presence of noncoherent noise. The ability of the randomly excited system to respond to the input signal frequency spectrum is determined by the complex transfer function (or frequency-

response function) $H(f)$ defined by

$$H(f) = \frac{G_{xy}(f)}{G_{xx}(f)} = \frac{S_{xy}(f)}{S_{xx}(f)}, \quad (\text{dimensionless}) \quad (1.22)$$

where

$$S_{xy}(f) = \int_{-\infty}^{\infty} R_{xy}(\tau) e^{-2i\pi f\tau} d\tau \quad [\text{V}^2/\text{Hz}] \quad (1.23)$$

and

$$S_{xx}(f) = \int_{-\infty}^{\infty} R_{xx}(\tau) e^{-2i\pi f\tau} d\tau \quad [\text{V}^2/\text{Hz}]. \quad (1.24)$$

Writing $H(f)$ in the polar coordinate form

$$H(f) = |H(f)| e^{-i\phi(f)} \quad (1.25)$$

it can be shown from (1.18), (1.19), and (1.25) that

$$|H(f)| = |G_{xy}(f)|/G_{xx}(f) \quad (1.26a)$$

and

$$\phi(f) = \theta_{xy}(f). \quad (1.26b)$$

The relationships shown in (1.26) are extremely important in stationary random photothermal wave systems, as they permit the evaluation of the complete frequency-response function of such systems, assumed linear, from cross-spectral measurements. Finally, the time-domain unit impulse response function $h(\tau)$ can be defined as the Fourier transform of the transfer function $H(f)$:

$$h(\tau) = \int_{-\infty}^{\infty} H(f) e^{2i\pi f\tau} df. \quad (1.27)$$

This function is of great importance to photothermal wave applications, as it can generate a system function mathematically equivalent to the system's response to a single ultrashort excitation pulse, by weighing the transfer function over the entire frequency spectral content of the actual random excitation.

B. Time-Delay-Domain Method and its Advantages for Dynamic System Measurements

In the previous section the time domain unit impulse response function $h(\tau)$ was defined to be the complex Fourier transform of the transfer function $H(f)$ of a photothermal wave system excited by white noise, i.e., a truly stationary random input signal. From (1.27) we can write:

$$H(f) = \int_{-\infty}^{\infty} h(\tau) e^{-2i\pi f\tau} d\tau. \quad (1.28)$$

This equation shows that a precise determination of the frequency response function of a system is intimately related to, and strongly dependent upon, the experimenter's ability to measure accurately the unit impulse response function of the system. This requirement, in turn, presupposes the use of wideband random noise as the excitation source with theoretical frequency content from DC to infinity. Such an excitation source function would be char-

acterized by a Dirac-delta-function-type autocorrelation function $R_{xx}(\tau)$, and a constant one-sided autospectral density function $G_{xx}(f)$ in the time and frequency domains, respectively [7]. Real experimental systems cannot, of course, generate purely random signals. Random noise generating devices (e.g., Bruel and Kjaer Model 1405) tend to generate pseudorandom signals, i.e., band-limited (wideband or narrowband) noise. Most realistic wideband random noise generators suffer from limited dynamic range properties and require sophisticated measurement equipment. The obvious alternative is the corresponding time domain method, i.e., pulsed laser excitation in the case of photothermal wave systems. This technique has been used extensively in recent years [8], [9]. From the point-of-view of system frequency response this method has the advantage of minimizing the required measurement time, but also suffers somewhat in measurement dynamic range properties [10]. Another potential disadvantage of the pulsed laser method is the possibility of material damage by the high energy fluxes delivered by the laser to the latter, which may rob a time-domain photothermal wave technique of its attractive nondestructive features.

Very recently [6], [11], [12] Mandelis *et al.* introduced the concept of a photoacoustic/photothermal excitation and detection technique intermediate between time and frequency domains. This technique is similar to the frequency modulation (FM) of communications systems. It was introduced by Heyser [13] in 1967 in the field of acoustical measurements of loudspeakers and was named time delay spectrometry (TDS) by the same author. Through its implementation and long-term use in acoustic engineering, TDS has been shown to outperform any other time selective technique with respect to noise rejection and nonlinearity suppression from measurements of systems with linear behavior [14]. The TDS technique, which is based on a linear frequency sweep of the excitation function, is akin to chirp modulation [15], [16]. It has been specifically compared to the impulse response transformation and the wideband (pseudo) random-noise methods and has been proven to have superior measurement dynamic range properties [10]. The reason for the excellent dynamic range characterizing TDS can be understood in regarding the measurement system to which the frequency-swept signal is applied as a transmission line. An important parameter of such a system is the total time delay τ_D required for the transmission of information from the input to its output. Primary consideration, therefore, must be given to minimizing the effective duration of a transmitted pulse. A relevant measure of this duration is T_D , the second moment of the power of the impulse response $h(\tau)$ about a suitably chosen origin τ_0 [14]:

$$T_D = \min_{-\infty < \tau_0 < \infty} \left(\int_{-\infty}^{\infty} \tau^2 |h(\tau - \tau_0)|^2 d\tau \right). \quad (1.29)$$

It can be shown [17] that T_D is minimized when

$$t_g(\omega_i) = \frac{d\phi_i(\omega_i)}{d\omega_i} = \text{constant} \quad (1.30)$$

where $t_g(\omega_i)$ is a group time delay in the classical wave mechanical sense and expresses the relative time shift of instantaneous signal frequency components $\omega_i = 2\pi f_i$ adjacent to a reference frequency [18]; and $\phi_i(\omega_i)$ is the instantaneous signal phase angle. Using the minimum transit time condition (1.30), the rate of change of the phase angle

$$\frac{d\phi_i(t)}{dt} = \frac{d\phi_i}{d\omega_i} \frac{d\omega_i}{dt} \quad (1.31)$$

is seen to involve the instantaneous signal frequency dependence on time, a concept incompatible with conventional Fourier transform theory, where the variables frequency f and time t are taken to represent physical phenomena in two mathematical domains, which are Fourier transforms of each other. Nevertheless, (1.30) and (1.31) show that as long as

$$\frac{d\phi_i(t)}{dt} = t_g \left[\frac{d\omega_i(t)}{dt} \right] \quad (1.32)$$

the effective duration of a transmitted pulse will be minimized. This network has been called a *minimum phase system* [19]. The minimization of the pulse duration (width) thus results in an extended transfer function (i.e., its Fourier transform, see (1.28)) dynamic range, a feature exploited in the recent work by Mandelis *et al.* [11], [12]. A minimum phase system can be shown to be a linear phase system [14], i.e.

$$d\omega_i(t)/dt = \text{constant}. \quad (1.33)$$

This implies that a sweep input signal can be any function of time $X(t)$ modulated between two extreme deviation frequencies such that the instantaneous value of the *frequency-like* quantity $f_i(t)$ is given by [13]

$$f_i(t) = \left(\frac{\Delta f}{T} \right) t + \frac{1}{2} (f_2 + f_1) \equiv \left(\frac{\Delta f}{T} \right) t + f_c. \quad (1.34)$$

In (1.34) $\Delta f = f_2 - f_1$ is the carrier signal modulation bandwidth, $f_c = (f_2 + f_1)/2$ is the average carrier frequency, and T is the total sweep period.

The sweep rate S is defined as the time derivative of the frequency-like quantity $f_i(t)$:

$$S = \frac{df_i(t)}{dt} = \frac{\Delta f}{T} \quad [\text{Hz/s}]. \quad (1.35)$$

S is independent of time, a general feature of linear sweep modulation systems that results directly from the linear dependence on time of (1.34). Assuming the excitation function to be a cosinusoidal carrier wave [10], [13], [14], a time-delay photothermal system input will be given by (Fig. 2)

$$X(t) = A(t) \cos [\phi_i(t)] \quad (1.36)$$

where $A(t)$ is the amplitude modulation (AM) function,

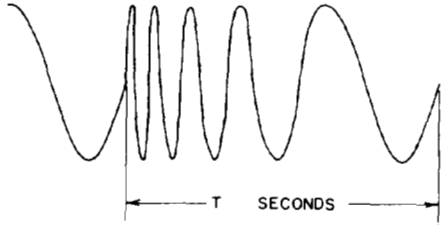


Fig. 2. Theoretical frequency-swept signal [13].

usually chosen to be constant. Taking t_g to be a time delay commencing at the initiation of the input signal [20], i.e., $t_g = t$ in (1.32), we find upon integration:

$$\begin{aligned}\phi_i(t) &= \int_0^t 2\pi q \left[\frac{df_i(q)}{dq} \right] dq + \phi_o \\ &= 2\pi \left(\frac{\Delta f}{2T} \right) t^2 + 2\pi f_c t + \phi_o \\ &= (\pi S) t^2 + \omega_c t + \phi_o\end{aligned}\quad (1.37)$$

where $\phi_o \equiv \phi_i(0)$ is the input phase at $t = 0$.

The experimental conditions chosen for photothermal wave measurements are [11], [12] $\phi_o = 0$ and $f_i = 0$ and $\phi_i(T + \delta t) = \phi_i(\delta t)$, for $\delta t \rightarrow 0$, where A is constant. These correspond to a linear saw-tooth frequency sweep between dc and $f_2 = f_{\max}$ with multiple repetitions of the sweep process every period T . Under these conditions, (1.36) can be conveniently written in the form [13]

$$X(t) = X_+(t) + X_-(t); \quad 0 \leq t \leq T \quad (1.38)$$

where

$$X_+(t) = \frac{A}{2} \exp [i(\pi S t^2 + \omega_c t)] \quad (1.39a)$$

and

$$X_-(t) = \frac{A}{2} \exp [-i(\pi S t^2 + \omega_c t)]. \quad (1.39b)$$

It can be shown [13] that the frequency swept signal component functions $\exp [\pm i(\pi S t^2)]$ in (1.39) can be expanded in conventional Fourier series

$$\exp [\pm i(\pi S t^2)] = \sum_{n=-\infty}^{\infty} C_{\pm N}^{\pm} e^{iN\omega_0 t} \quad (1.40)$$

with [6], [13]

$$\begin{aligned}C_{\pm N}^{\pm} &= \frac{1}{T} \left(\frac{1}{2S} \right)^{1/2} \\ &\cdot [C(\omega_{\max}) \pm iS(\omega_{\max})] \exp [\mp i(N\omega_0)^2/4\pi S]\end{aligned}\quad (1.41)$$

where $C(x)$ and $S(x)$ are the Fresnel cosine and sine integrals [21], respectively, and $\omega_0 \equiv 2\pi/T$.

The importance of the Fourier expansions in (1.40) and (1.41) lies in that they enable the experimenter to determine analytically the frequency content of the swept wave along with the weighting factors $C_{\pm N}^{\pm}$, which ultimately

give the frequency bandwidth of the Fourier transform of the input signal.

The signal generated using the linearly swept wave $X(t)$ of (1.38) is a special case of the more general class of phase-angle-modulated systems [22]. In this context the time-delay photothermal excitation can be regarded as similar to a frequency modulated (FM) wave, with the time integral of the applied swept wave

$$m(t) = 2\pi \int_0^t \left(\frac{\Delta f}{T} \right) q dq \quad (1.42)$$

in (1.37) acting as the FM wave modulating the baseband signal f_c . In either case the instantaneous frequency $f_i(t)$ is the sum of the time-varying component and the unmodulated carrier wave f_c .

II. PSEUDORANDOM TECHNIQUES AND WINDOWING IN PHOTOTHERMAL WAVE SIGNAL GENERATION

Truly stationary random signals with a probability density function given by (1.9) (white noise) have the property that their autocorrelation function is a Dirac delta function

$$R_{xx}(\tau) = \delta(\tau). \quad (2.1)$$

This property suggests that the noise contains equal amounts of all frequencies, which is unrealistic in practice because it requires an infinite bandwidth. In general, it suffices to specify the frequency band of interest and within that band determine a level power spectrum. Random-noise signals with a finite bandwidth can be generated by physical means, such as the noise obtained from the random behavior of gaseous discharges of semiconductor materials [23]. These physical methods suffer, however, from their unrepeatability, which implies very long sampling time intervals to establish small variance values. The undesirable disadvantage of long computational times can be overcome by use of a repeated pattern of random noise having a predetermined power spectrum and amplitude probability distribution. This is defined as pseudorandom noise. The probability density of such pseudorandom signals can be made very close to the Gaussian (1.9). In performing spectral analysis of pseudorandom signals, a serious problem is that of leakage due to the finite frequency interval. Leakage is a result of the inability of the analysis to recognize harmonic components whose periods are not integer factors of the predetermined frequency bandwidth. Such components will be eliminated as much as possible. Another problem appears with the large variances of autospectral density functions computed from the numerical Fourier transformation of the autocorrelation function (1.13). To minimize the variance it is necessary to carry out some averaging operation (smoothing out) usually through a pre-selected weighting function. Furthermore, a trade-off between increasing the spectral width of the weighting function which decreases the variance, and an increasing degree of biasing of the computed spectrum exists. A compromise smoothing window, which reduces variance

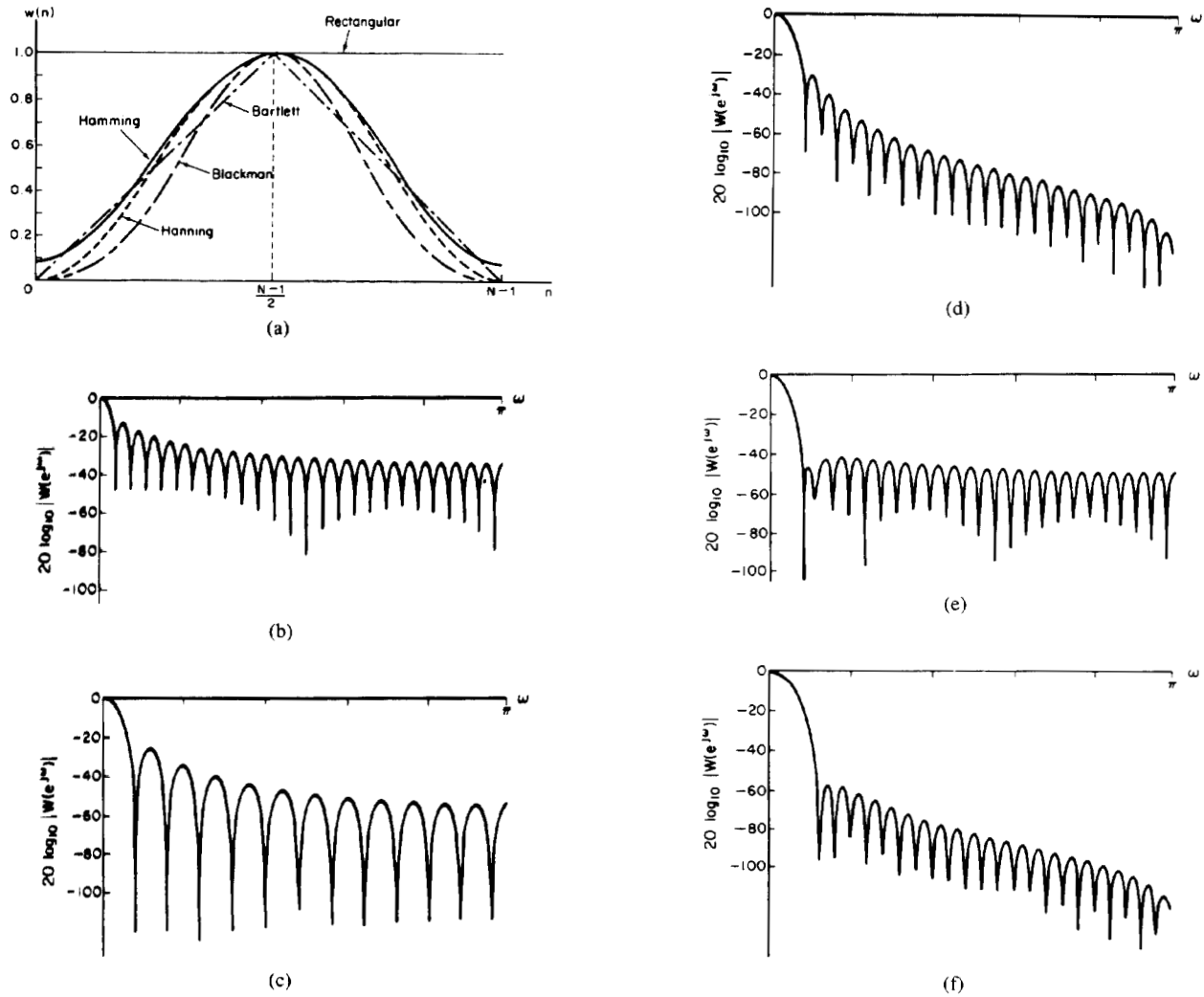


Fig. 3. (a) Commonly used windows for FIR filter design. (b)-(f) Fourier transforms of these windows: (b) Rectangular. (c) Bartlett (triangular). (d) Hanning. (e) Hamming. (f) Blackman [24].

without overbiasing the spectral features and can also suppress leakage is usually imposed during the spectral analysis of pseudorandom noise excited systems. The most common windows available for, and used with, photothermal wave systems are finite impulse response (FIR) filters. These are linear windows designed to obtain a finite-duration impulse response sequence. Examples of some commonly used FIR filters are shown in Fig. 3. In this figure $W(e^{j\omega})$ is the transfer function of the window [24]:

$$W(e^{j\omega}) = \sum_{n=0}^{N-1} e^{-j\omega n} = \left[\frac{\sin(\omega N/2)}{\sin(\omega/2)} \right] e^{-j\omega[(N-1)/2]} \quad (2.2)$$

where N is the total number of samples of the Fourier transform taken experimentally ($N = 51$ in Fig. 3). The various windows are defined by their finite duration shape $w(n)$ in the time domain as follows [25].

1) Rectangular:

$$w(n) = 1, \quad 0 \leq n \leq N - 1. \quad (2.3a)$$

2) Bartlett:

$$w(n) = \begin{cases} \frac{2n}{N-1}, & 0 \leq n \leq \frac{N-1}{2} \\ 2 - \frac{2n}{N-1}, & \frac{N-1}{2} \leq n \leq N-1. \end{cases} \quad (2.3b)$$

3) Hanning:

$$w(n) = \frac{1}{2} \left[1 - \cos\left(\frac{2\pi n}{N-1}\right) \right], \quad 0 \leq n \leq N-1. \quad (2.3c)$$

4) Hamming:

$$w(n) = 0.54 - 0.46 \cos\left(\frac{2\pi n}{N-1}\right), \quad 0 \leq n \leq N-1. \quad (2.3d)$$

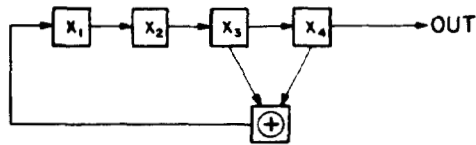


Fig. 4. A maximum-length linear shift register [26].

5) Blackmann:

$$w(n) = 0.42 - 0.5 \cos\left(\frac{2\pi n}{N-1}\right) + 0.08 \cos\left(\frac{4\pi n}{N-1}\right), \quad 0 \leq n \leq N-1. \quad (2.3)$$

For FIR and other linear windows of pseudorandom input signals it can be shown [26] that

$$S_{yy}(f) = |w(f)|^2 S_{xx}(f) \quad (2.4)$$

i.e., the output power spectrum $S_{yy}(f)$ is determined upon multiplication of the input power spectrum $S_{xx}(f)$ by the square of the absolute value of the filter transfer function. It is due to (2.4) that signal filtering can take place during spectral processing. There are, however, some disadvantages to linear filtering [27].

The most widely used digital pseudorandom techniques in photothermal wave applications to-date, are derived from pseudorandom binary sequences (PRBS). These sequences are generated as two level signals using shift register techniques [26], [28], [29]. The most popular PRBS in photoacoustics has been one based on maximum-length sequences (m -series) [30], for which $N = 2^n - 1$, where N is an odd integer and n is an arbitrary integer. An example of the shift register corresponding to an m -series is shown in Fig. 4. The sequence is generated by the shift register of degree $n = 4$, whose feedback logic is the parity check function on the positions x_3 and x_4 . In Fig. 4 this function is denoted by \oplus and is known as the *mod 2 sum* function given by the truth table:

mod 2 sum	0	1
0	0	1
1	1	0

If the initial state of the shift register is 1 0 0 0 (reading from left to right), then the succession of states will be: [1 0 0 0], [0 1 0 0], [0 0 1 0], [1 0 0 1], [1 1 0 0], [0 1 1 0], [1 0 1 1], [0 1 0 1], [1 0 1 0], [1 1 0 1], [1 1 1 0], [1 1 1 1], [0 1 1 1], [0 0 1 1], [0 0 0 1], and [1 0 0 0]. The shift register output (the last position of each state) will thus be

$$000100110101111 \quad (2.5)$$

repeating periodically with period 15 ($N = 15$). The thus formed m -series PRBS can be used to modulate the exciting light beam intensity in a photoacoustic experiment. The first such sequence from a shift register of degree n

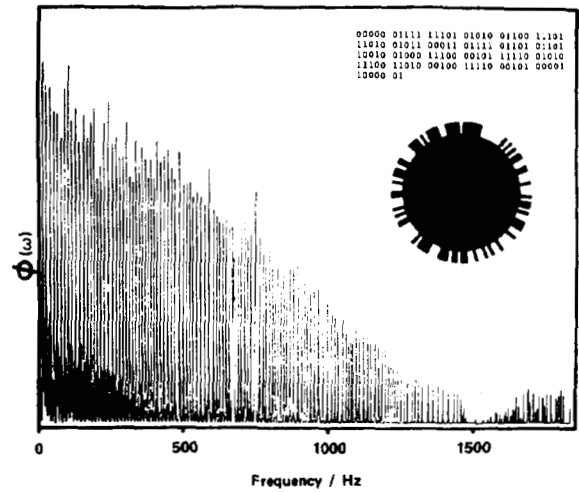


Fig. 5. An m -series PRBS with repetition period $N = 127$ corresponding to a shift register of degree 7 ($127 = 2^7 - 1$), as well as the silhouette of the photoacoustic mechanical chopper and input one-sided autospectral density $\phi(\omega) = G_{xx}(f)$. The chopper cut-outs correspond to the indicated sequence [30].

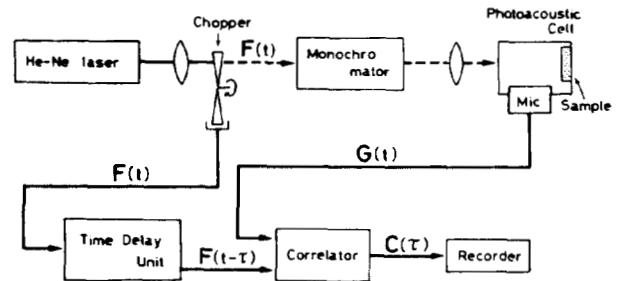


Fig. 6. Block diagram showing the measuring apparatus for cross-correlation photoacoustic spectroscopy. PRBS optical excitation can be induced monochromatically as shown ("first kind"), or with a broadband light source, e.g. a Xenon lamp ("second kind") [30].

= 5 and pseudo-period $N = 31$ was used by Kato *et al.* [31] to fabricate a mechanical chopper. A more complex light chopper with $N = 127$ and $n = 7$ was subsequently used by Sugitani *et al.* [30] and is shown in Fig. 5. These mechanical choppers were used with a photoacoustic apparatus similar to conventional frequency domain photoacoustic spectroscopy [39], with the exception that an analog cross-correlator and a time-delay device (a micro-computer) replaced the lock-in detection (Fig. 6). An experimental apparatus utilizing PRBS light modulation, such as the one shown in Fig. 6, exhibits the following properties [33]: 1) the signal intensity I_0 has only two levels (on I_0 ; off 0) and may switch from one level to the other only at time intervals $t = 0, \lambda, 2\lambda, \dots$; 2) the PRBS is a deterministic sequence because it is predetermined whether the signal will change level at any particular interval by the construction of the chopper; 3) the PRBS pseudo-period T_0 is given by $T_0 = N\lambda$, where N is an odd integer; 4) in any one pseudo-period T_0 , there are $\frac{1}{2}(N + 1)$ intervals at one level and $\frac{1}{2}(N - 1)$ intervals at the other level; 5) the autocorrelation function $R_{xx}(\tau)$ is triangular with a base-width equal to two sampling periods (Fig. 7): it thus represents an approximation to the ideal Dirac delta function required for a flat autospectral

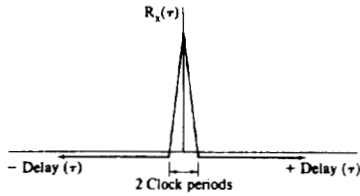


Fig. 7. Autocorrelation function of a PRBS signal [23].

density (Wiener theorem, (1.13)). Mathematically, however, an m -series PRBS remains quite different from purely white noise, its distribution probability density given by the binomial distribution due to the existence of two discrete signal levels I_0 and 0, and the fact that these levels are mutually exclusive:

$$P(X) = \frac{N!}{X!(N - X)!} \left[\frac{1}{2} \left(1 + \frac{1}{N} \right) \right]^X \left[\frac{1}{2} \left(1 - \frac{1}{N} \right) \right]^{N-X} \quad (2.6)$$

where $P(X)$ is the probability density that the signal will be in the "on" state exactly X times during one pseudo-period of a PRBS chopper. The probability that at any time interval the signal will be "on" is

$$p = \frac{1}{2} (N + 1)/N = \frac{1}{2} \left(1 + \frac{1}{N} \right). \quad (2.7)$$

The appendix lists a simple Fortran program for the generation of an m -series PRBS with a specific example for $n = 9$ and $N = 511 (= 2^9 - 1)$. It appears to be mechanically awkward to fabricate PRBS choppers for photoacoustic applications using shift registers of degree larger than five. If such a series is desirable, acoustooptic or electrooptic modulators are a far better choice. Kirkbright *et al.* [34] appear to be the first group of investigators who reported using acoustooptic modulation of the intensity of a Krypton ion laser from an internal PRBS generator of a signal processor (Solartron Model 1200) in photoacoustic applications. Mandelis *et al.* [12] used a similar idea in a photothermal beam deflection application with a home-made PRBS voltage generator.

Coufal *et al.* [5], [35], [36] have applied multiplex excitation methods to photoacoustic imaging applications. Some of these methods involve very interesting spatial Hadamard [35] and spatial Fourier [36] transformations of signals obtained by sample excitation through special surface masks. These spatial transform methods will not be discussed further in this article which is entirely concerned with time and frequency-domain multiplexing of pseudorandom excitation signals. Coufal [5], [37] used a random number sequence generated by the linear congruential method [38] to excite photoacoustic and photothermal signals in solids. Fig. 8 shows the resulting random signal and its one-sided autospectral density function. The linear congruential method produces linear congruential sequences of random numbers $\langle X_n \rangle$ by setting

$$X_{n+1} = (aX_n + c) \text{ mod } (m), \quad n \geq 0 \quad (2.8)$$

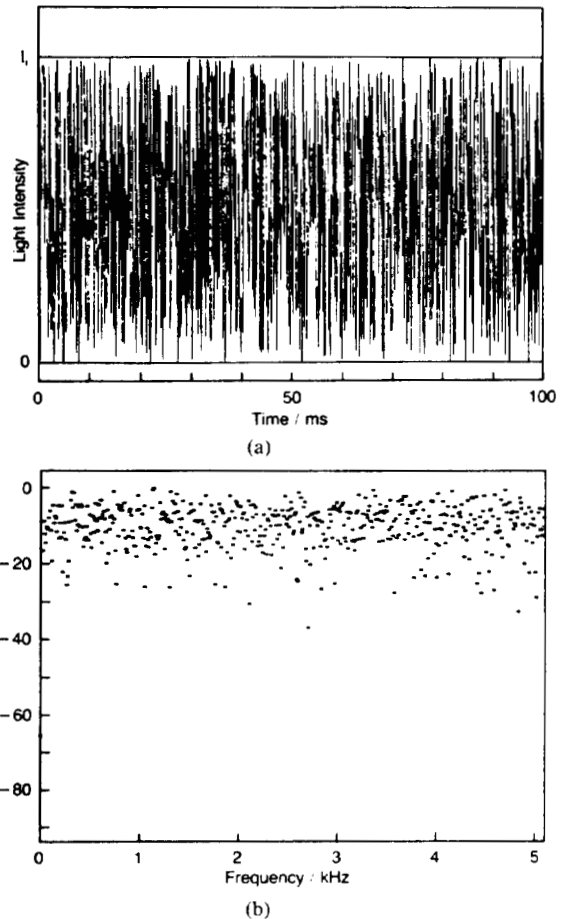


Fig. 8. (a) Pseudorandom noise generated by the linear congruential method. (b) One-sided autospectral density function (power spectrum) of (a) [5].

where

- m modulus, $m > 0$;
- a multiplier, $0 \leq a \leq m$;
- c increment, $0 \leq c \leq m$; and
- X_0 starting value, $0 \leq X_0 \leq m$.

Thus the sequence obtained when $m = 10$ and $X_0 = a = c = 7$ is 7, 6, 9, 0, 7, 6, 9, 0, \dots . The generated sequences are only pseudorandom, forming periods ("loops") of numbers which are repeated endlessly. This property is common to all sequences of the general form $X_{n+1} = f(X_n)$ [38]. The crucial step in (2.8) is finding "good" values for the number m , which should be rather large, since the period can have at most m elements. A complete discussion of the proper choices of the modulus and the multiplier for fast pseudorandom sequence generation can be found in [38]. Furthermore, other important random number generating schemes such as quadratic congruential methods, additive number generators and the combination of random number generators are also discussed in some depth by Knuth. The intensity trace of Fig. 8(a) can thus be understood considering that Coufal [5], [37] used acoustooptic modulation of a He-Ne laser beam, so that the intensity modulation amplitude was presumably proportional to the value of a random number

generated by the linear congruential sequence at a specific instant.

III. PHOTOACOUSTIC AND PHOTOTHERMAL APPLICATIONS OF PSEUDORANDOM OPTICAL EXCITATION PROCESSES

A. Non-spectroscopic Applications

Most pseudorandom optical excitation photoacoustic nonspectroscopic studies to-date have focused on thermal imaging applications and the determination of thermal parameters of materials. Sugitani *et al.* [30] used the *m*-series PRBS mechanical chopper of Fig. 5 with the experimental apparatus shown in Fig. 6 to study layered structures, such as glass plates covered with various coatings. Fig. 9 is a sequence of numerically computed cross-correlation functions $C(\tau) \equiv R_{xy}(\tau)$ (see (1.12)) from samples with polyethylene coatings of varying thicknesses. These authors named the monochromatic probing of layered structures via PRBS photoacoustic spectroscopy "correlation spectra of the first kind." Excitation of these materials was induced by a 50 mW He-Ne laser. The polyethylene films were transparent at 632.8 nm and the observed variable peak delay time τ_0 was interpreted as a thermal diffusion delay time for the energy absorbed by the painted glass to appear at the surface of the films. The shape of the curves and the broadening with increased thickness were identified as the mathematical equivalent of the impulse response function for the system. Theoretically, the interpretation of the cross-correlation function $R_{xy}(\tau)$ as the impulse response $h(\tau)$ of a randomly excited system can be justified under a rather stringent condition [6]: substituting (1.22) into (1.27) gives

$$h(\tau) = \int_{-\infty}^{\infty} \left[\frac{S_{xy}(f)}{S_{xx}(f)} \right] e^{2\pi i f \tau} df \quad (3.1)$$

A comparison of (3.1) to the cross-correlation function, given by the Fourier transform of $S_{xy}(f)$ in (1.23):

$$R_{xy}(\tau) = \int_{-\infty}^{\infty} S_{xy}(f) e^{2\pi i f \tau} df \quad (3.2)$$

shows clearly that the cross-correlation function is equal to the unit impulse response of the system only in the special event of a uniform auto-spectrum of the input function $X(t)$, i.e., only if

$$S_{xx}(f) = 1. \quad (3.2')$$

The above equation is strictly valid when the autocorrelation function of the input is a Dirac delta function. Fig. 5 shows the experimental autospectral density function (power spectrum) of the mechanical chopper used by Sugitani *et al.* Fig. 10 also shows the input autocorrelation and one-sided autospectral density function of a chopper identical to the one in Fig. 5 [39]. In both figures the non-flat power spectra and the broadened autocorrelation spike in Fig. 10 indicate that caution should be exercised in the interpretation of curves such as those of Fig. 9. For a

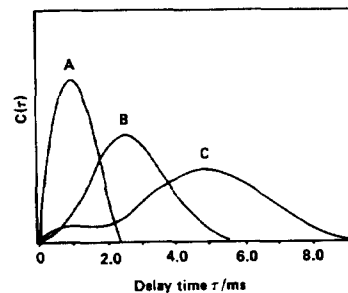


Fig. 9. Cross-correlation functions $C(\tau) \equiv R_{xy}(\tau)$ from sheets of polyethylene films coated on a glass plate sprayed with blue paint. Film thickness: A = 0 μm ; B = 30 μm ; and C = 60 μm [30].

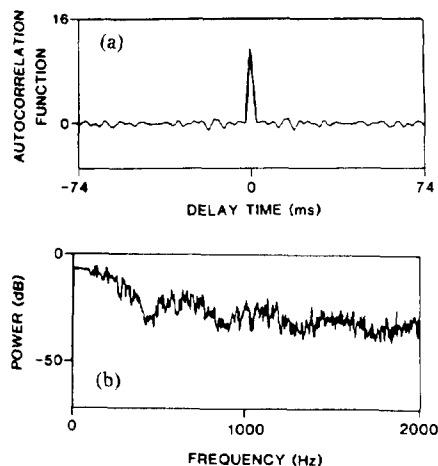


Fig. 10. Autocorrelation function (a) and one-sided autospectral density function (b) of an *m*-sequence PRBS chopper identical to the one presented in Fig. 5 [39].

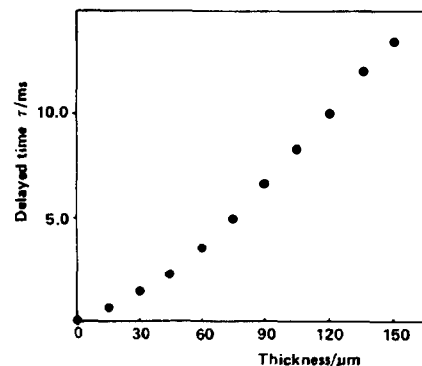


Fig. 11. Peak delay time τ_0 vs. thickness from sheets of polyethylene films coated on a glass plate sprayed with blue paint [30].

purely heat diffusive process the peak delay time of the photoacoustic impulse response is expected to be proportional to the square of the film thickness l when the film is transparent to the exciting radiation [40]:

$$\tau_0 = \left(\frac{e_s}{e_b} \right)^2 \frac{l^2}{\alpha_s} \quad (3.3)$$

where e_s , e_b are the thermal effusivities of the film and its backing, respectively, and α_s is the thermal diffusivity of the film. Fig. 11 is the experimental functional dependence between τ_0 and l for the various polyethylene film

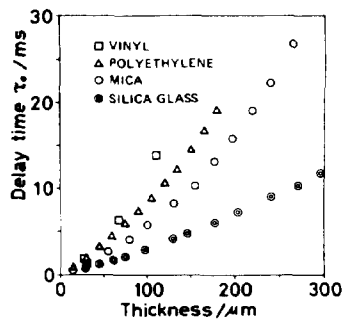


Fig. 12. Peak delay times vs. thickness from vinyl, polyethylene, mica, and silica glass films coated on a backing plate sprayed with paint acting as a thermal resistance [41].

thicknesses measured by Sugitani *et al.* [30]. It is apparent from this figure that τ_0 depends on some power b of l , $b > 1$. Fig. 12 shows similar results obtained from essentially the same photoacoustic system as shown in Fig. 6 by Uejima *et al.* [41]. These curves were numerically fitted, using the method of least squares, to the equation

$$\tau_0 = a \left(\frac{1}{\alpha_s} \right) l^b + c \quad (3.4)$$

where a , b , and c are constants to be determined by the fit. Satisfactory agreement between the glass data and (3.4) was reported for the following set of parameters: $a = 4 \times 10^5$, $b = 1.33$, and $c = 0.65$, using the measured value for the thermal diffusivity $\alpha_s = 6.0 \times 10^{-3} \text{ cm}^2/\text{s}$. The authors invoked the effect to thermal contact resistance between the sample and backing, a space occupied by the sprayed paint on the backing, in order to explain the $b = 1.33$ power dependence of τ_0 on l . They further developed a one-dimensional heat conduction model, which gave satisfactory fits to the data curves upon adjustment of the interfacial thermal contact resistance values.

Blackbody photoacoustic correlograms generated with an m -series PRBS optical excitation have been studied in some detail due to their importance as a system response reference. In the early work by Kato *et al.* [31] and Sugitani *et al.* [30], the cross-correlation function between the input optical and output photoacoustic signals of carbon black was recorded and found to exhibit consistently a non-zero peak delay time τ_0 . Taking into account that $\tau_0 > 0$ cannot be attributed to thermal diffusion processes, since light absorption and conversion to heat is essentially a surface process for carbon black, a certain amount of speculation has appeared in the literature. For their $N = 31$, $n = 5$ PRBS chopper, Kato *et al.* [31] attributed τ_0 to the time lag between a heat pulse generation at the sample surface and the attainment of the highest air pressure in the volume of the photoacoustic cell. These authors observed that $\tau_0 \approx 2 \text{ ms}$ was independent of the carbon black grain size and fitted the decay profile of $R_{xy}(\tau)$ to the exponential function $\exp[-(\tau - \tau_0)/\tau_R]$, with a fitting value of $\tau_R = 6 \text{ ms}$. They also attributed the probable origin of

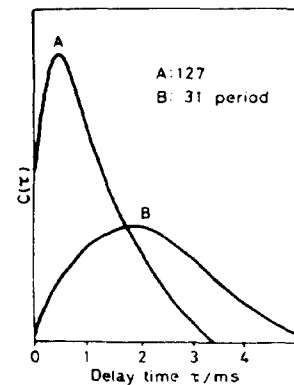


Fig. 13. Cross-correlation function $C(\tau) = R_{xy}(\tau)$ of photoacoustic signals from a carbon black sample, using a 127-bit (A) and 31-bit (B) chopper rotated at 396 rpm. [42].

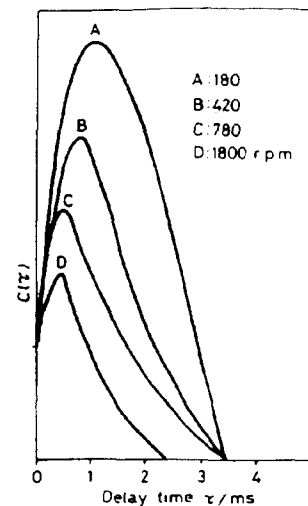


Fig. 14. Cross-correlation function $C(\tau) = R_{xy}(\tau)$ of photoacoustic signals from the same carbon black sample, recorded with a 127-bit PRBS chopper at rotational speeds of 180 rpm (A); 420 rpm (B); 780 rpm (C); and 1800 rpm (D) [42].

the grain-size independent τ_R to the cooling characteristics of the inner-cell gas. Sugitani *et al.* [30] made similar observations regarding the grain-size independence of τ_0 in correlograms obtained with an $N = 127$, $n = 7$ PRBS chopper. In this case, however, $\tau_0 = 0.46 \text{ ms}$. Sugitani and Uejima [42] further studied the dependence of the photoacoustic cross-correlation function from carbon black on the period N and the rotational speed of the PRBS chopper. Their findings are shown in Figs. 13 and 14.

Similar trends to those of Fig. 14 were also observed by Mandelis and Dodgson [43] with slightly different τ_0 values from those of Sugitani and Uejima [42], which were attributed to the somewhat different experimental and data processing apparatus. Mandelis and Dodgson presented a one-dimensional theoretical heat conduction model of the pseudorandom photoacoustic signal and calculated the expected peak delay time τ_0 of the cross-correlation function for a blackbody. Fig. 15 shows the comparison of the theory with experimental data from 100-percent India ink with an $N = 127$, $n = 7$ PRBS chopper [44]. The substantial discrepancy between the two curves

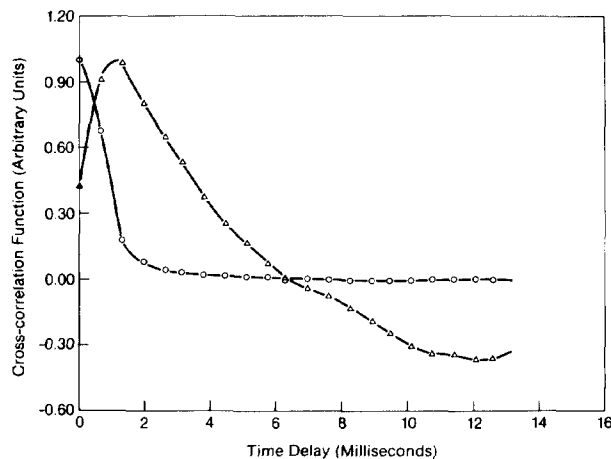


Fig. 15. Experimental (dash-triangle line) and theoretical (dash-circle) photoacoustic cross-correlation from 100-percent India ink [44].

demonstrates quantitatively the nonthermal diffusion origin of the one-dimensional blackbody cross-correlation peak delay time. Mandelis and Dodgson [43] suggested that the observed discrepancy regarding the value of τ_0 is due to the experimental apparatus itself, notably the roll-off in the microphone frequency response above ~ 10 kHz, which coincided with the earliest measurable cross-correlation delay times τ . A qualitative consideration of the RC time constant of the microphone ($\tau_{RC} \approx 30$ ms for the 1/8" B&K condenser microphone model 4138) tended to raise the theoretical τ_0 of Fig. 15 above the zero level and toward the peak of the experimental curve. The above discussion shows that it is desirable to obtain better delay time resolution in PRBS photoacoustics, a fact which can be most easily achieved using a large period N modulator with broadband photoacoustic detection transducers other than the gas-coupled microphone cell. Kirkbright *et al.* [34], [45] used PRBS acoustooptic modulation employing the PRBS signal generated in a digital signal analyzer (Solartron Instruments Ltd., UK, Model 1200). Unfortunately, these authors used a conventional gas-coupled microphone photoacoustic cell, which tends to reduce the high frequency response and mechanical noise-free advantage built into the acoustooptic modulation of laser beams, due to the band-limited microphone response. Very recently Mandelis *et al.* [12] performed the first reported m -series PRBS photothermal beam deflection (PDS) experiments using a homemade PRBS waveform generator programmed with $N = 127$, $n = 7$ sequence to modulate the $1.06 \mu\text{m}$ beam from a 2 W $\text{Nd}^{3+}:\text{YAG}$ laser through an acoustooptic modulator. The expanded laser beam was used to excite thermal waves in a blackbody in contact with water, and the He-Ne probe laser beam deflection was monitored through a gigahertz-bandwidth detector consisting of a pinhole and photodiode in series. Fig. 16 shows the impulse response peak delay time τ_0 vs. the square of the probe beam offset x_0^2 . The data were obtained with a Nicolet 660A Dual-Channel FFT Analyzer. From the slope the thermal diffusivity of water was calculated and was found to be in reasonable agreement

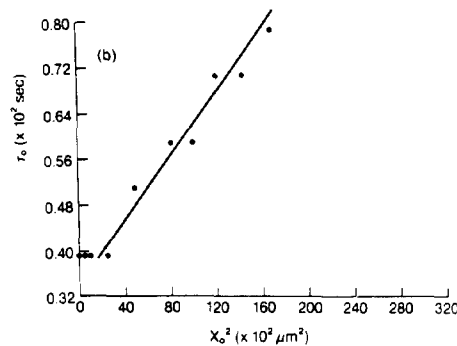


Fig. 16. PRBS spectrometer impulse response peak delay time dependence on photothermal beam deflection probe beam offset above a blackbody (anodized aluminum) surface [12].

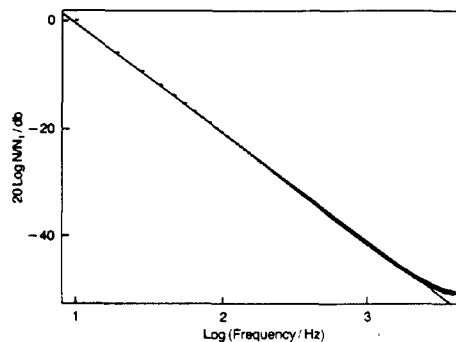


Fig. 17. Transfer function of a thermally thin carbon loaded polymethyl methacrylate (PMMA) used as a test sample, determined from the frequency domain data generated by noise modulation of the incident light intensity [5].

with the published value of $1.4 \times 10^{-3} \text{ cm}^2/\text{s}$. The essentially linear (albeit with a somewhat large scatter) dependence of τ_0 on x_0^2 and the reasonable value for $\alpha_{\text{H}_2\text{O}}$ obtained from Fig. 16 indicate that elimination of band-limited response detection devices is necessary for the correct interpretation of data, such as the data agreement with a simple heat conduction mechanism. Coufal [5] had similar success in interpreting the random noise transfer function $H(f)$ of carbon loaded poly (methyl methacrylate) (PMMA) films deposited on a wide-bandwidth pyroelectric thin-film calorimeter [46], [47] in terms of the Rosenzweig-Gersho model [48] (See Figs. 17 and 18).

Kirkbright and Miller [45] performed a careful study of the depth-profiling capabilities of PRBS photoacoustics by measuring the cross-correlation function's delay-time dependence of photoexcited two- and three-layered samples consisting of thin polyester films coated on the back surface with black ink and subsequently mounted onto a card substrate. Some of the samples were further coated on the front surface with a thin layer of red pigment. The photoacoustic responses under different excitation lines of a Krypton ion laser for the three-layered system are shown in Fig. 19. The sharp peak of curve A exhibited at early times is indicative of the presence of the pigment, which absorbs strongly the 568-nm radiation; the relatively weak amplitude of the first peak shown in curve B under 647-nm excitation indicates that the pigment is a weak absorber at that wavelength, while the second broad peak

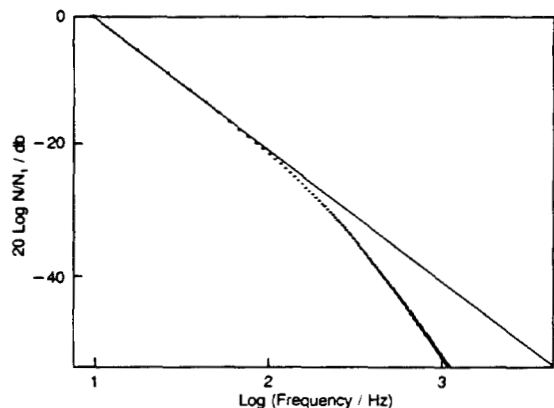


Fig. 18. Transfer function of a PMMA sample showing the transition from thermally thin to thermally thick in the frequency range probed by the noise modulation of Fig. 8(a) [5].

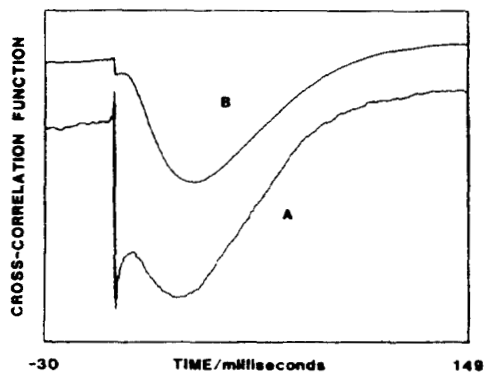


Fig. 19. Cross-correlation/impulse response function for a three-layer sample consisting of an absorbing substrate, 50 μm of polyester film, and a thin top layer of red pigment: Photoacoustic response obtained by using (A) the Kr⁺ 568 nm (yellow-green) laser line and (B) the 647 nm (red) laser line [45].

remained essentially unaffected. This latter peak was associated with the substrate black ink layer, which is an equally strong absorber of both wavelengths. Fig. 19 demonstrates the important point that frequency multiplexed photoacoustic methods can yield depth-selective information along a time-delay axis. This kind of information can, in principle, also be obtained via dispersive techniques such as lock-in detection upon measurement of the signal phase angle [49]. The time required for the acquisition of similar amounts of information is, however, considerably longer than the multiplexed technique. Furthermore, Kirkbright and Miller pointed out that the dispersive methods cannot resolve signals from thermal sources (e.g., defects) overlapping spatially. The significance of plots such as Fig. 19 lies in the simplicity of their interpretation as impulse responses. Earlier on we discussed the theoretical conditions under which a cross-correlation function may be interpreted as an impulse response measurement. Kirkbright and Miller [45] verified this equivalence for their multilayered measurements by comparing the sample response to a single short pulse from the internal impulse generator of their Solartron 1200 signal analyzer to the cross-correlation function, and showing that the two pulse profiles were essentially iden-

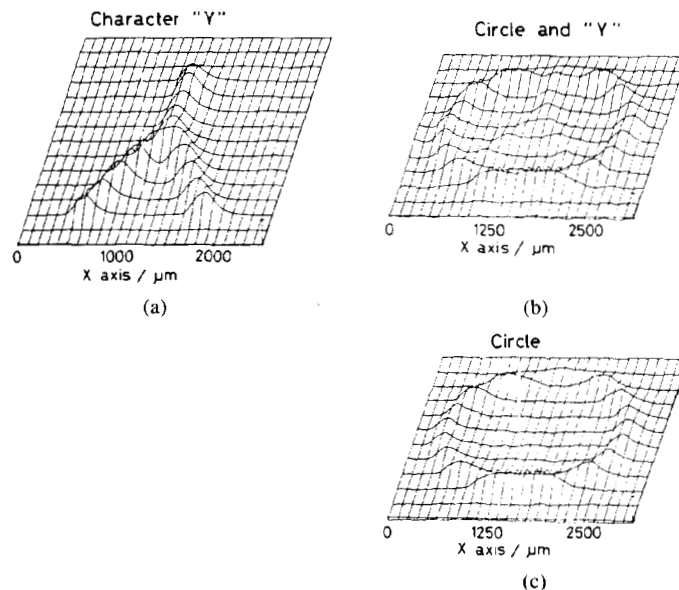


Fig. 20. Cross-correlation photoacoustic imaging of model sample (see text) obtained with a $N = 255$, $n = 8$ PRBS chopper. The delay times are fixed at (a) 0.5 ms; (b) 3.8 ms; and (c) 4.3 ms [50].

tical under their experimental conditions. Sugitani and Uejima [50] recently applied PRBS photoacoustics to pattern recognition in a structure where a polyvinylidene chloride film with a pattern (the letter Y) was superposed over a base of the same material with a different pattern (a circle). Between the two sheets a third unpatterned polyvinylidene chloride sheet was inserted, and the composite structure was scanned with the 632.8-nm beam of a 20-mW (minimum power) He-Ne laser. The results shown in Fig. 20 demonstrate the depth-profiling abilities of PRBS photoacoustics via the characteristic correspondence between depth fixing and delay-time fixing. Kirkbright *et al.* [34] obtained subsurface defect information in aluminum via a similar surface line scan technique using a Kr⁺ ion laser.

Very recently [51], Miller presented a one-dimensional digital model based on the discretization of time and space coupled with a finite difference approximation to the heat diffusion equation

$$\frac{\partial T}{\partial t} = \alpha_s \frac{\partial^2 T}{\partial x^2} \tag{3.5}$$

The above equation was expressed in a finite difference form:

$$\Delta T_j = \alpha_s \frac{\Delta t}{\Delta x^2} (T_{j+1} - 2T_j + T_{j-1}) \tag{3.6}$$

where ΔT_j is the fractional temperature change due to heat transfer for the j th element of a phase. Heat transfer across inhomogeneous interfaces was calculated using [52]

$$\Delta T_i = \frac{2\Delta t}{(\Delta X_a + \Delta X_b)} \left(\frac{\alpha_b}{\Delta X_b} \right) (T_{i+1} - T_i) - \left(\frac{\alpha_a}{\Delta X_a} \right) (T_i - T_{i-1}) \tag{3.7}$$

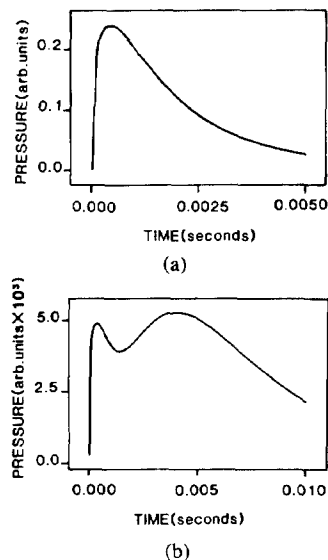


Fig. 21. Simulation of the photoacoustic impulse response for (a) an opaque sample and (b) a two-layer absorbing system. The model results are in agreement with experimental response characteristics with a discrepancy in the absolute value of the peak delay time [51].

where i is the space element containing the boundary between regions (a) and (b). Fig. 21(a) shows simulations of the photoacoustic impulse response for an opaque sample. Fig. 21(b) shows simulations from a two-layer absorbing system. This model, based on purely heat diffusional processes, appears to have the potential for much needed quantitative analysis of PRBS photoacoustic depth-profiling signals from samples with spatially variable thermal diffusivities. It predicts, however, system response factors 2–4 times faster than the experimental data and thus shares this common characteristic with the analytical spectroscopic model developed by Mandelis and Dodgson [43]. Miller [51] has recognized the need for the incorporation of the microphone transfer function to the model for quantitative comparisons, as was pointed out earlier in the Time Domain investigations by Mandelis and Royce [53].

In conclusion, it appears at this time that the depth-profiling abilities of PRBS photoacoustics have been demonstrated with definite advantages over frequency-domain dispersive methods, primarily in terms of time savings in signal acquisition and simplicity of interpretation of impulse response data. Signal-to-noise ratios (SNR) comparable to lock-in detection have been claimed [45]. When compared to single pulse response in a single experiment, the PRBS impulse response exhibited an order of magnitude higher SNR [45]; however, the single pulse method has the advantage of minimizing the required measurement time [10], [45].

B. Spectroscopic Applications

The majority of spectroscopic applications using pseudorandom optical excitation to-date has appeared in efforts to identify different chemical species lying at some depth from a sample surface. The identification, mostly qualitative, is performed through the spectral signature of

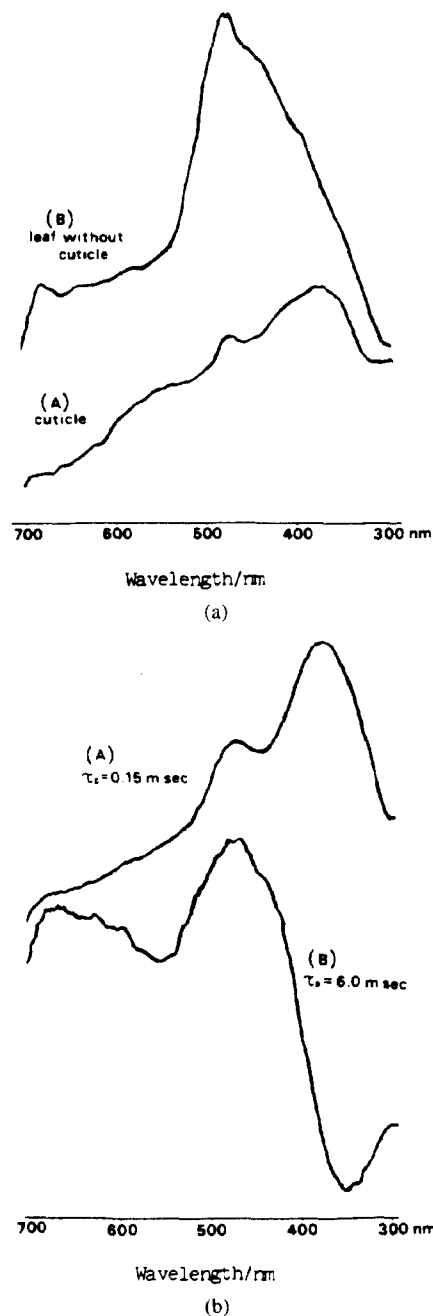


Fig. 22. (a) Ordinary photoacoustic spectra of spinach leaf with the cuticle intact (A) and without the cuticle (B). (b) Cross-correlation photoacoustic spectra of the whole leaf of spinach at fixed delay times: $\tau_D = 0.15$ ms (A); $\tau_D = 6.0$ ms (B) [31].

the underlayer obtained at some predetermined delay time τ_D of the cross-correlation function, upon comparison with the (known) frequency-domain photoacoustic spectrum corresponding to the underlayer in question. Historically, Sugitani named this mode of cross-correlation photoacoustics "spectra of the second kind" [30]. Fig. 22 demonstrates the general features of the technique [31]: the photoacoustic spectra of Fig. 22(a) were taken with a conventional frequency-domain gas-coupled microphone apparatus using a spinach leaf with the cuticle intact (curve A); and the leaf without the cuticle (curve B). The pronounced absorption at ~ 350 nm of curve A is indicative

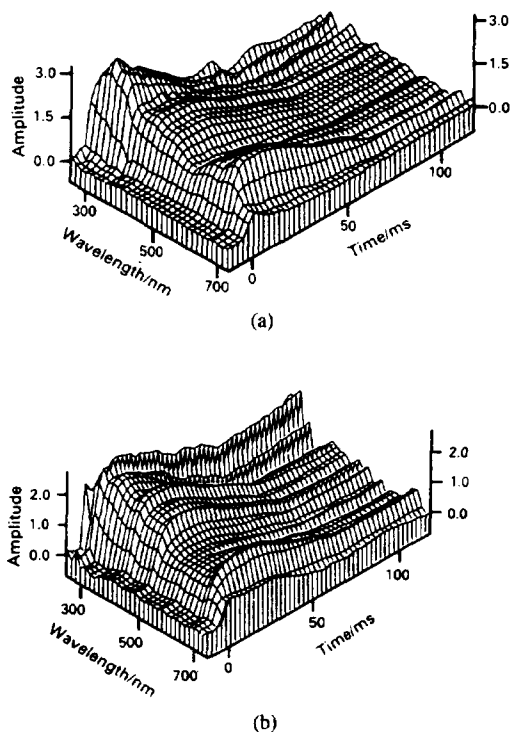


Fig. 23. Isometric projections of cross-correlation photoacoustic data obtained from (a) whole lettuce leaf and (b) from a whole lettuce leaf sprayed with dilute sulphuric acid ($\text{pH} = 3$) (acid rain) [54].

of the protection to the leaf body from UV radiation provided by the overlying cuticle. The large absorptions at around 470 nm and 670 nm observed in curve *B* are due to the use of solar energy by the exposed leaf for carrying out its photosynthetic processes. Fig. 22(b), curve *A*, is a PRBS spectrum of the whole leaf with the cuticle intact at the fixed delay time $\tau_D^{(A)} = 0.15$ ms. At this early time the photoacoustic spectrum obtained reflected the spectral features of a thin surface layer, with the cuticle characteristics (peak at ~ 350 nm) most pronounced. When a longer delay time $\tau_D = 6.0$ ms was considered, curve *B*, the spectral features of the underlying leaf become pre-eminent, with the resulting spectrum exhibiting a peak at ~ 470 nm and a broader peak at ~ 670 nm. This example shows the definite merit of pseudorandom-generated spectra in offering depth-resolved information of different absorbing layers *without* the need to strip the surface layer as was the case with conventional frequency-domain photoacoustic spectroscopy. Similar applications, with PRBS optical excitation and scanning the wavelength range, were subsequently reported using chromatophores such as poinsettia leaves, which consist of a transparent epidermis layer and a mesophyll layer with chlorophyll cells [30]. Kirkbright *et al.* [39] further examined bulk-dyed polymer films of polyurethane acrylate and polyvinyl chloride with and without surface coatings, lettuce and laburnum leaves [54] under conditions of exposure or not to Paraquat (a herbicide). These authors reported three-dimensional spectra of cross-correlation amplitude vs. optical wavelength with delay time along the third (depth) axis. An example of such a surface, called an "isometric pro-

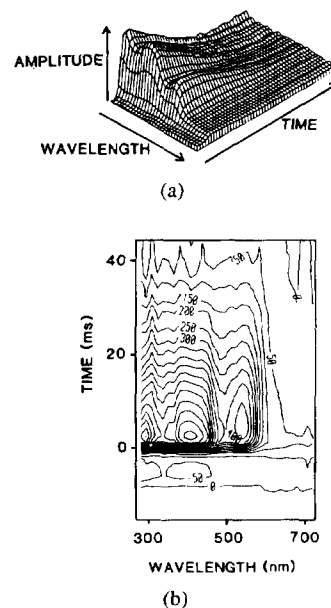


Fig. 24. Cross-correlation/impulse response photoacoustic data for a matrix of polyvinylchloride heavily doped with bromothymol blue. The sample was planar and approximately 1 mm in thickness. (a) Isometric projection. (b) Contour map [39].

jection," is shown in Fig. 23. The juxtaposition of these surfaces gives information about surface reactions: In the healthy leaf of Fig. 23(a), a strong UV absorption arising from the surface cuticle and a long-wavelength absorption band arising from the chlorophyll is evident. The latter band is broad, as the chlorophyll is held by the subsurface cells in a number of different chemical environments. The effect of simulated acid rain (sulphuric acid at $\text{pH} = 3$) after overnight exposure and attack of the cell membranes is clear in Fig. 23(b): there is partial dissolution of the surface cuticle and rupture of the subsurface cells. These events resulted in a diminution of the amplitude of the cross-correlations/impulse responses in the UV region, which were directly attributed to the chemical degradation of the cuticle and subsurface cellular membranes. This degradation process was found to destroy the binding sites within the subsurface cells, thus rendering all of the plant chlorophyll chemically equivalent. This resulted in a sharpening of the chlorophyll absorption feature having a maximum of ~ 680 nm, together with the disappearance of the absorption shoulder at ~ 600 nm.

While the concept of isometric projections of the data had been previously introduced by Sugitani *et al.* [30], Kirkbright *et al.* [39], [54] introduced another useful method of spectroscopic data presentation, namely a quantitative contour map of the data in which computer-generated contours pass through points of equal amplitude Fig. 24: this figure reveals some features otherwise masked in isometric projection surfaces. For instance, 1) the absorption feature centered at 280 nm is more intense than that at 412 nm and 2) the distribution of absorption throughout the sample changes from band to band. It is clear from the contour map that for the absorption peak at 560 nm, light penetrates more deeply into the sample than

at the other absorption peaks. Recently, Uejima *et al.* [55] extended the spectroscopic depth-resolving power of PRBS-optical excitation-induced photoacoustic spectroscopy to the investigation of multilayer photographic color reversal films. They used Fujichrome 100 color film with essentially five layers: a protective layer *A*, 2.7 μm thick; a yellow layer *B*, 7.2 μm ; a magenta (red) layer *C*, 4.5 μm ; a cyan (blue) layer *D*, 4.5 μm ; and a substrate film-base layer *E*. By choosing the appropriate delay times of their "second kind" cross-correlation spectra, these authors were able to demultiplex (resolve) the various spectral peaks due to the four layers *A*, *B*, *C*, and *D*. These spectra, produced with $\tau_D = 0.04$ ms (*A*), 0.4 ms (*B*), 1.2 ms (*C*), and 2.4 ms (*D*) were found to be in qualitative agreement with conventional photoacoustic spectra taken of each layer individually. This interesting application is an excellent demonstration of the wealth of depth-resolved data that can be obtained with the pseudorandom technique nondestructively, a difficult or impossible task for frequency-domain PAS due to 1) the large attenuation of bulk signals [32], [48] and poor SNR at high modulation frequencies and 2) poor resolution of overlapping spectral features [49] suffered by the lock-in detection technique.

A very recent and interesting application of the spectroscopic capabilities of cross-correlation/impulse response PRBS photoacoustic spectroscopy to the monitoring of time-dependent kinetic phenomena in physico-chemical systems has been reported by Miller *et al.* [56]. In that work PRBS intensity modulation of the 647-nm line of a Kr^+ ion laser was effected using an acousto-optic modulator producing a 127-bit sequence, which was provided by the waveform generator of a Prosser Scientific Instruments Ltd., UK, Model A08 correlator. The system used was a blue, solvent-based ink absorber in contact with a transparent waterproof sealing plastic film (Parafilm by Gallenkamp, UK), which allowed the underlying ink to diffuse forward at a rate low enough to allow several pseudorandom measurements to be taken during the course of the experiment with an average of 30–50 measurements per time interval (20 to 35 s). Photoacoustic signal cross-correlations/impulse responses were calculated using a Solartron 1200 digital signal analyzer. Typical results are shown in Fig. 25, which is a plot of 30 averages of the cross-correlation functions from seven readings taken at three-minute intervals. It can be observed that the broad secondary peak of the correlogram moves closer to the primary stationary peak and its relative amplitude increases with increasing time from the start of the experiment. This trend can be interpreted by an optical energy absorption/thermal energy conversion mechanism at the subsurface chromophore (ink)-surface film interface: as the ink diffuses forward and closer to the surface, the thermal wave signal from the advancing interface responsible for the photoacoustic response gradually shifts to earlier delay times, as expected. The signal amplitude also increases, as a larger fraction of the generated heat reaches the approaching upper film surface, with proportionately

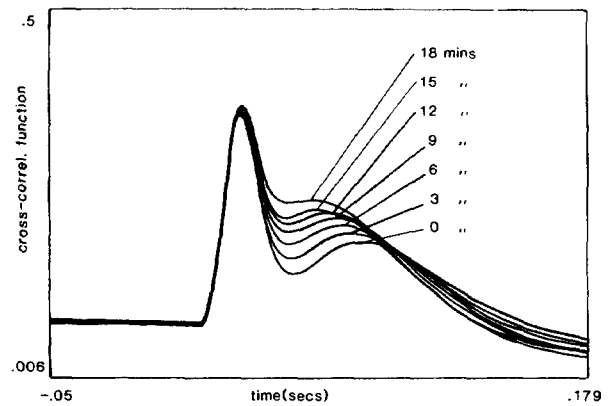


Fig. 25. Cross-correlation functions from kinetic experiments with small amounts of ink placed under a plastic film [56].

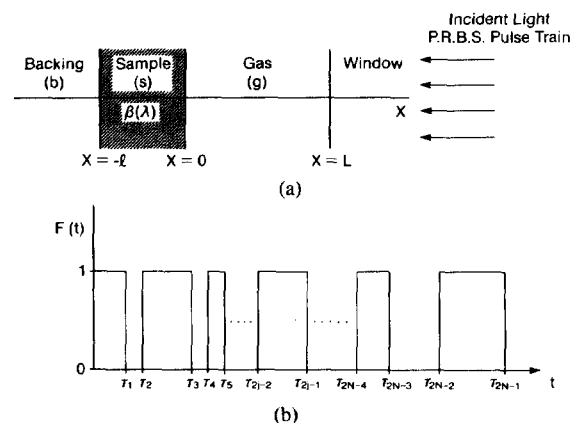


Fig. 26. (a) One-dimensional geometry of correlation photoacoustic (CPAS) sample cell for theoretical model. (b) Theoretical normalized PRBS optical excitation wavetrain incident on the sample. Total number of pulses in sequence is $N = 127$; duration of the j th pulse is $\Delta\tau_j = \tau_{2j-1} - \tau_{2j-2}$ [43].

less heat conduction to the backing material (a thermally thick [48] substrate). The excellent control of the peak delay time τ_0 , which was shown in [56] to be intimately related to the chromophore diffusion rate toward the surface, should allow a high degree of flexibility and quantitative analysis in future diffusion studies. With the exception of the recent work by Miller [51], however, all of the spectroscopic work discussed so far in this chapter is purely qualitative; even Miller's finite difference approach to the governing diffusion equation does not take the effect of variable optical absorption coefficients of materials into account explicitly. The first attempt to bridge this analytical gap and to show the spectroscopic relevance of PRBS photoacoustic spectroscopy in a quantitative fashion was made by Mandelis *et al.* [43], [44]. These authors developed a one-dimensional theoretical model in which the cross-correlation function between a PRBS input waveform and the theoretical photoacoustic output was numerically evaluated for condensed phase systems of variable optical absorption coefficients. The model system involved the solution of heat diffusion equations with a pseudorandom thermal forcing function $F(t)$ in the absorbing sample of the geometry shown in Fig. 26(a). For the important special case of photoacous-

tic detection at times short compared to the thermal diffusion time through the volume of the photoacoustic cell, and with a microphone transducer RC time constant τ_{RC} small compared to the earliest time at which signals would be detectable, the theoretical correlation photoacoustic (CPAS) response voltage was found to be [43]:

$$V(t; \tau_\beta) \approx GY(\beta) \tau_\beta \times \begin{cases} \sum_{j=1}^{N-1} Z[(t - \tau_{2j-1})/\tau_\beta] - Z[(t - \tau_{2j-2})/\tau_\beta] + Z(0) - Z[(t - \tau_{2N-2})/\tau_\beta], & \tau_{2N-2} \leq t \leq \tau_{2N-1} \\ \sum_{j=1}^N Z[(t - \tau_{2j-1})/\tau_\beta] - Z[(t - \tau_{2j-2})/\tau_\beta], & t \geq \tau_{2N-1}. \end{cases} \quad (3.8)$$

The PRBS optical wavetrain input was expressed as (Fig. 26(b)):

$$F(t) = \sum_{j=1}^N f_j(t)$$

where

$$f_j(t) = \begin{cases} 1, & \tau_{j-1} < t < \tau_j \\ 0, & \tau_j < t < \tau_{j+1}. \end{cases} \quad (3.9)$$

In (3.8) the following definitions were made:

$$Z(x) \equiv e^x \operatorname{erfc}(\sqrt{x}) \quad (3.10)$$

G is a constant dependent on microphone parameters; $Y(\beta) \propto \beta$ a constant dependent on sample parameters and linearly varying with the absorption coefficient β ; and $\tau_\beta \equiv 1/\beta^2 \alpha_s$ is a thermal diffusion delay time from a depth in the sample equal to the optical absorption length β^{-1} . The input-output cross-correlation function

$$R_{FV}(\tau; \tau_\beta) = \lim_{T \rightarrow \infty} \frac{1}{2T} \int_{-T}^T F(t) V(t + \tau; \tau_\beta) dt \quad (3.11)$$

was calculated using the discretized formula [33]

$$R_{FW}(\tau_r; \tau_\beta) = R_{FV}(\tau_r; \tau_\beta) + R_{Fn}(\tau_r) \quad (3.12)$$

where R_{FW} is the cross-correlation function in the presence of acoustic noise in the system and R_{FV} is the discretized cross-correlation function of interest

$$R_{FV}(\tau_r; \tau_\beta) = \frac{1}{(j-r)} \sum_{k=1}^{j-r} F_k \cdot V_{k+r} \quad (3.13)$$

where

$$\tau_r = r/\text{SR} \quad (3.14)$$

and

$$r = 0, 1, 2, \dots, Q. \quad (3.15)$$

SR is the sampling rate used in the data acquisition routine, and Q is the number of cross-correlations calculated. R_{Fn} is the input cross-correlation function with noise $n(t)$. As $F(t)$ and $n(t)$ are statistically independent from each other in the limit $T \rightarrow \infty$, it is expected that $R_{Fn} \rightarrow 0$, i.e.

$$R_{FW}(\tau_r; \tau_\beta) = R_{FV}(\tau_r; \tau_\beta), \quad T \rightarrow \infty \quad (3.16)$$

This theory was further tested experimentally using solid materials (Ho_2O_3 powders [43]) and liquids (inks of variable concentration [44]). The apparatus used is shown in Fig. 27. The thermal diffusivity of Ho_2O_3 powders was measured using well-established frequency-domain photoacoustic techniques [57]. These measurements showed

that Ho_2O_3 powders behaved photoacoustically essentially like a one-dimensional continuous solid, with the added advantage of a large SNR due to the small size of the powders. The effective optical absorption coefficient $\beta(\lambda)$ of Ho_2O_3 was then calculated using results from a recent work [58]. First, the conventional frequency-domain and PRBS-induced photoacoustic spectra were compared between ~ 410 nm and 520 nm, and they were found to be identical within the standard deviation of the apparatus (Fig. 28). This agreement indicates the absence of any significant spectral distortion in the PRBS spectrum. Second, the predetermined optical absorption coefficient spectral profile $\beta(\lambda)$ was used as a numerical input for τ_β in the theory of (3.8)–(3.15). The results are shown in Fig. 29 at 8 nm resolution. The agreement between experiment and theory is very good except for the highest β values, and indicates that the theory as formulated by Mandelis and Dodgson can adequately describe the spectroscopic capabilities of CPAS. The departure of the theoretical curve from the data points at high β was attributed to the difference between the values of β used in the model and the actual rapidly changing with wavelength β values, which could not be accurately determined with the 8-nm-resolution spectrometer. It thus appears that the results obtained in [43] establish the PRBS-induced photoacoustic response as a quantitative spectroscopic technique. Fig. 30 shows spectroscopic results from the PRBS apparatus of Fig. 27 using water-diluted India ink samples with known optical absorption coefficients at 632.8 nm. The β range is broader than that calculated for Ho_2O_3 [43]. The magnitude curve exhibits photoacoustic saturation at high β and an essentially linear dependence of the PRBS cross-correlation function peak magnitude of β at low values of this parameter, in agreement with the Rosencwaig-Gersho theory [48]. The peak delay time curve tends to saturation for high β values too; this tendency is, however, more gradual than the peak magnitude and can be compared to a frequency-domain analogous phenomenon involving the saturation of photoacoustic amplitude and phase [59]. The increase in τ_0 with decreasing β observed in Fig. 30(b) is consistent with the longer thermal delay time τ_β required for heat produced in the bulk of the liquid to reach the gas-liquid interface at longer absorption lengths β^{-1} . The β -dependence of τ_0 was found to be.

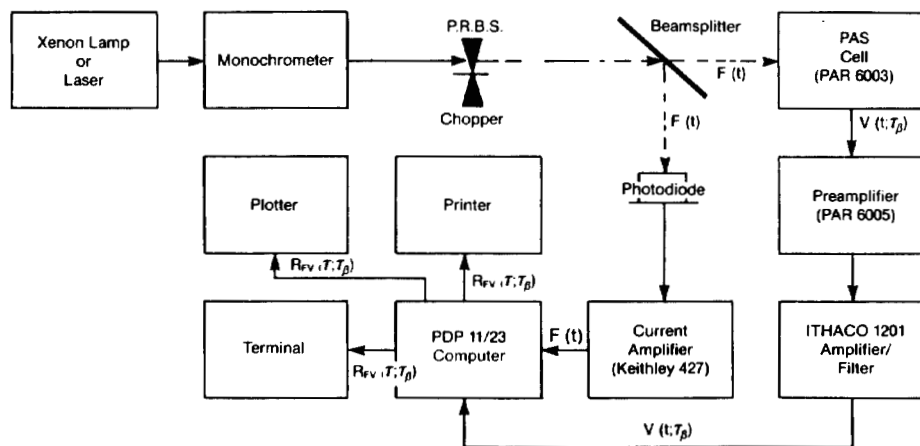


Fig. 27. CPAS microphone-gas coupled experimental apparatus [44].

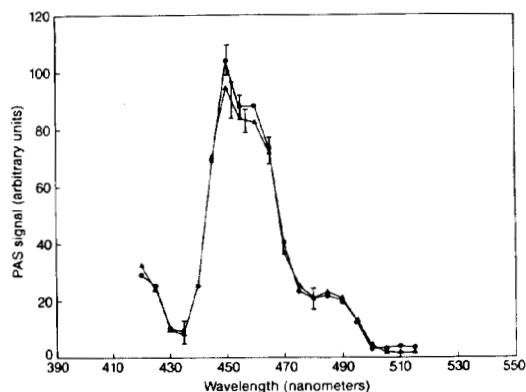


Fig. 28. Frequency-Domain PAS (triangle) amplitude at 50 Hz and cross-correlation PAS (dot) magnitude at 6 rps. Both curves were artificially matched at 440 nm [43].

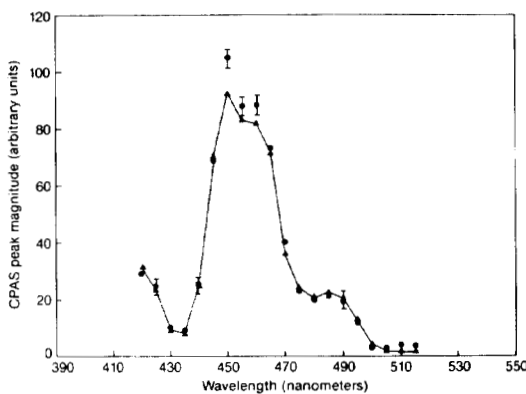


Fig. 29. Wavelength dependence of the CPAS magnitude of H_2O_3 at the peak delay time τ_0 . The dots and triangles respectively denote the experimental and theoretical results.

however, more complicated than the, perhaps expected, β^{-2} . The data of Fig. 15 were also obtained using the 100-percent India ink and the theoretical model of (3.8–3.15). Aside from the large discrepancy in the absolute values of the peak delay times which was discussed in Part A of this chapter, a microphone “flyback” feature is also prominent at $\tau > 6$ ms, yielding negative experimental cross-correlations. This feature was also observed by other workers [45] and can be ultimately traced to the mechanical inertia of the microphone diaphragm [60].

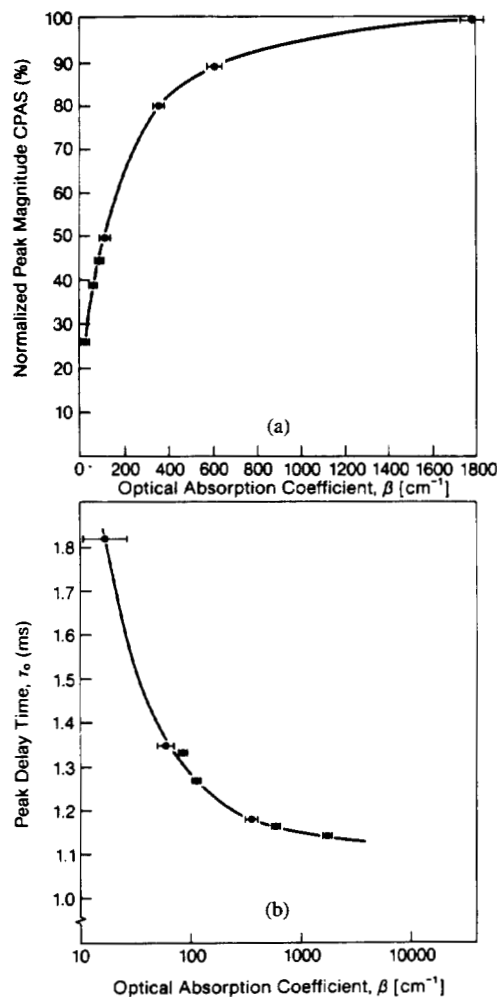


Fig. 30. Normalized CPAS signal as a function of aqueous ink solution β . (a) Peak magnitude. (b) Peak delay time [44].

At this time it is clear that the demonstrated depth-resolution capability of pseudorandom photoacoustic spectroscopy via the fixed delay time/fixed depth correspondence of spectroscopic features coupled with its ability for quantitative spectroscopy, will prove an invaluable tool for future investigations, such as subsurface species identification, kinematic studies of chemical reactions, and nondestructive chromophore characterization.

IV. FREQUENCY-MODULATED (FM) TIME-DELAY-DOMAIN TECHNIQUES IN PHOTOTHERMAL WAVE SIGNAL GENERATION

In the frequency swept optical excitation mode, the photoacoustic/photothermal wave information contained in the output signal response of the system can be recovered using the correlation and spectral analysis techniques presented in Section I-A. The definitions of the pertinent functions (1.11) and (1.12), however, must be extended to the complex domain to be able to accommodate analytically the FM input signals (1.32)–(1.41), which are themselves complex functions of time. This is easily accomplished by redefining the autocorrelation function (1.11)

$$R_{xy}(\tau) = \lim_{T \rightarrow \infty} \frac{1}{T} \int_0^T X^*(t) X(t + \tau) dt \quad (4.1)$$

and the cross-correlation function (1.12)

$$R_{xy}(\tau) = \lim_{T \rightarrow \infty} \frac{1}{T} \int_0^T X^*(t) Y(t + \tau) dt. \quad (4.2)$$

In (4.1) and (4.2) starred quantities indicate complex conjugation. The time-dependent signals obtained via correlation and convolution analysis using the FM mode of excitation carry information related to the delay of the output signal with respect to the input. It is therefore customary [13], [22] to use the variable τ instead of t for time and refer to the signal temporal evolution process in the time-delay domain. It is well known [13] that the complex output of a dynamic photothermal system $Y(t)$ is given as the convolution integral between the complex FM input signal and the unit impulse response function $h(t)$ of the system, provided the latter is assumed to be time-invariant

$$Y(t) = \int_0^{\infty} h(\tau) X(t - \tau) d\tau \quad (4.3a)$$

$$\equiv h(t) * X(t) \quad (4.3b)$$

where a causal relationship between input and system response was assumed, so that the lower limit of the integration was set to zero, rather than $-\infty$. Using (4.2) and (4.3), the following important relationship can be shown [6]:

$$R_{xy}(\tau) = h(\tau) * R_{xx}(\tau). \quad (4.4)$$

Once the autocorrelation function of the input is determined, the cross-correlation function between input and output can be calculated immediately from the known impulse response of the photothermal wave system. For the specific excitation function of (1.38) it can be shown that [6]:

$$R_{xy}(\tau) \approx h(\tau) * [R_{x+x+}(\tau) + R_{x-x-}(\tau)] \quad (4.5)$$

with

$$R_{x+x+}(\tau) = \frac{1}{4} \left(\frac{T - |\tau|}{T} \right) \left[\frac{e^{+2\pi i S \tau (T - |\tau|)} - 1}{2\pi i S \tau (T - |\tau|)} \right] \cdot \exp \{ i\pi \tau (2f_c + S|\tau|) \} \quad (4.6a)$$

and

$$R_{x-x-}(\tau) = \frac{1}{4} \left(\frac{T - |\tau|}{T} \right) \left[\frac{e^{-2\pi i S \tau (T - |\tau|)} - 1}{-2\pi i S \tau (T - |\tau|)} \right] \cdot \exp \{ -i\pi \tau (2f_c + S|\tau|) \}. \quad (4.6b)$$

The main advantage of the FM time-delay domain technique over both the impulse-response transformation (pulsed laser) method and the wideband random noise methods is its superior dynamic range. For a system or device in which the frequency response exhibits a resonance with a characteristic bandwidth Δf_R centered at f_0 , the maximum value of the Fourier transform of the transient time response of the system to an impulsive type of excitation (theoretically, a Dirac delta-function) is given by [10]

$$[F_{IR}(f)]_{\max} = F_{IR}(f_0) = \frac{1}{\pi} X_{\text{peak}} \left(\frac{\Delta f_M}{\Delta f_R} \right) \quad (4.7)$$

where X_{peak} is the maximum amplitude of the transient response, and $\Delta f_M = 1/T_M$ with T_M the pulse recirculation time. For a typical fast-Fourier-transform (FFT) signal-analyzer frequency resolution of, e.g., $3\Delta f_M = \Delta f_R$, (4.7) gives

$$F_{IR}(f_0) = \frac{1}{3\pi} X_{\text{peak}}. \quad (4.8)$$

If the input signal is of the frequency swept type and given by (1.36) with $A(t) = X_{\text{peak}}$, then at the resonant frequency f_0 the maximum value of the Fourier transform of the FM response is

$$F_{FM}(f_0) = X_{\text{peak}}. \quad (4.9)$$

From (4.8) and (4.9) it can be seen that, for an instrumental frequency resolution requirement of $\Delta f_M = \Delta f_R/3$, the difference in available dynamic range between a frequency sweep measurement and an impulse response transformation measurement on the same singly resonant test system is of the order of

$$20 \log_{10} \left[\frac{F_{FM}(f_0)}{F_{IR}(f_0)} \right] \approx 20 \text{ dB}. \quad (4.10)$$

In the FM mode Δf_M is defined as the inverse of the sweep period: $\Delta f_M = 1/T$. Fig. 31 shows a comparison between frequency response functions of a multiresonant system measured by the two techniques, where the superior dynamic range of the FM technique is clearly demonstrated. If wideband random noise is used as the input signal to the test system, the maximum value of the Fourier transform can be shown to be [10]

$$F_{RN}(f_0) = \frac{1}{3} \left(\frac{\Delta f_M}{\Delta f_R} \right)^{1/2} X_{\text{peak}} \quad (4.11)$$

where Δf_M now is the maximum root-mean-square (rms) value of the measured noise bandwidth centered at f_0 . For $\Delta f_M/\Delta f_R = \frac{1}{3}$, the loss in dynamic range compared to the FM technique is

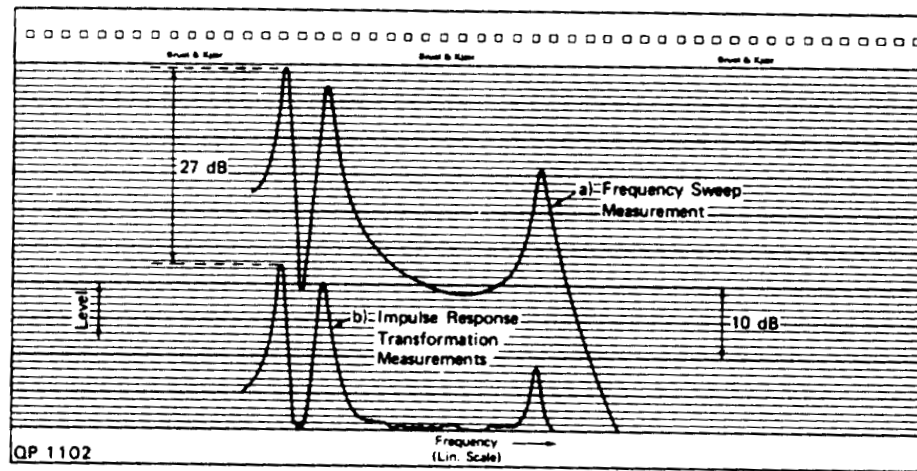


Fig. 31. The frequency response function of a multiresonant device [10].

$$20 \log_{10} \left[\frac{F_{FM}(f_0)}{F_{RN}(f_0)} \right] \approx 15 \text{ dB}. \quad (4.12)$$

This value corresponds quite closely to actually measured results. For a linear frequency sweep, a requirement for good spectral resolution is that the sweep rate (1.35) through a resonance f_0 with bandwidth Δf_R must satisfy

$$S \leq (\Delta f_R)^2. \quad (4.13)$$

This relation is tantamount to an instrumental "uncertainty principle" of the form

$$(\Delta f_R)(\Delta t) \geq 1. \quad (4.14)$$

Hence

$$S = \lim_{\Delta t \rightarrow 0} \frac{\Delta f_R}{\Delta t} \leq (\Delta f_R)^2.$$

V. PHOTOTHERMAL WAVE APPLICATIONS OF THE FREQUENCY-MODULATED TIME-DELAY-DOMAIN TECHNIQUE

The first reported photothermal wave system with FM time-delay-domain optical excitation is the recent photothermal deflection spectroscopic (PDS) apparatus of Mandelis *et al.* [6], [11], [12] shown in Fig. 32. These authors investigated the performance of the PDS apparatus using a blackbody reference sample (anodized aluminum) in water, as well as thin quartz films of variable thickness. A fast beam position detector was fabricated using a pinhole-photodiode arrangement with a 34 ns response time. The excitation beam from a 2 W Nd³⁺:YAG pump laser was expanded over the sample in order to facilitate the (one-dimensional) theoretical interpretation of the data. Frequency modulation of the pump beam intensity was effected using an HP 3325A Synthesizer/Function Generator. The system output was registered as a photovoltage whose amplitude was proportional to the spatial deflection of the He-Ne probe beam due to the Mirage effect [61]. All the necessary frequency and time-delay-domain functions were calculated via a Nicolet Scientific Corp. Model 660A dual channel FFT analyzer. The

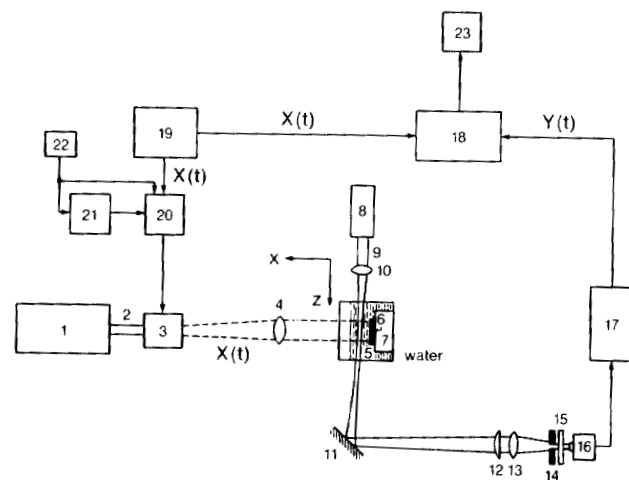


Fig. 32. FM time-delay mirage effect spectrometer. 1) Nd³⁺:YAG pump laser. 2) CW 1.06 μm beam. 3) Acousto-optic (A/O) modulator. 4) Alignment lens. 5) Water. 6) Sample. 7) Sample holder. 8) He-Ne probe laser. 9) 632.8-nm probe beam. 10) Focusing lens. 11) Optical lever reflector mirror. 12 and 13) Lenses. 14) 50- μm diameter pinhole. 15) He-Ne beam interference filter. 16) Fast risetime photodiode. 17) Wide bandwidth preamplifier. 18) Dual channel FFT analyzer. 19) Synthesizer/function generator. 20) A/O modulator driver. 21) A/O driver power amplifier. 22) A/O modulator power supply. 23) Computer memory storage [11].

magnitude and phase of the complex transfer function $H(f)$ of the blackbody/water interface is shown in Fig. 33(i). These data were taken between dc ($f_1 = 0$) and 1280 Hz ($= f_2$ in (1.34)) with $T = 0.41$ s and a sweep rate $S = 3.122$ kHz/s applied to the acousto-optic modulator. Correlation and spectral processing, averaged over 1000 frequency sweeps with 1024 data points per sweep, required approx. 6–7 min. This time can be reduced, however, to be as low as 1 min, corresponding to a minimum number of ~ 200 sweeps/average. This time is by far shorter than the time required to obtain the same information dispersively using lock-in detection as in Fig. 33(ii). The reliability of the data shown in Fig. 33(ii) is, furthermore, inferior to that of Fig. 33(i), as the mean of only 20 samples per average was taken over 14 data points. From this comparison it was concluded that the

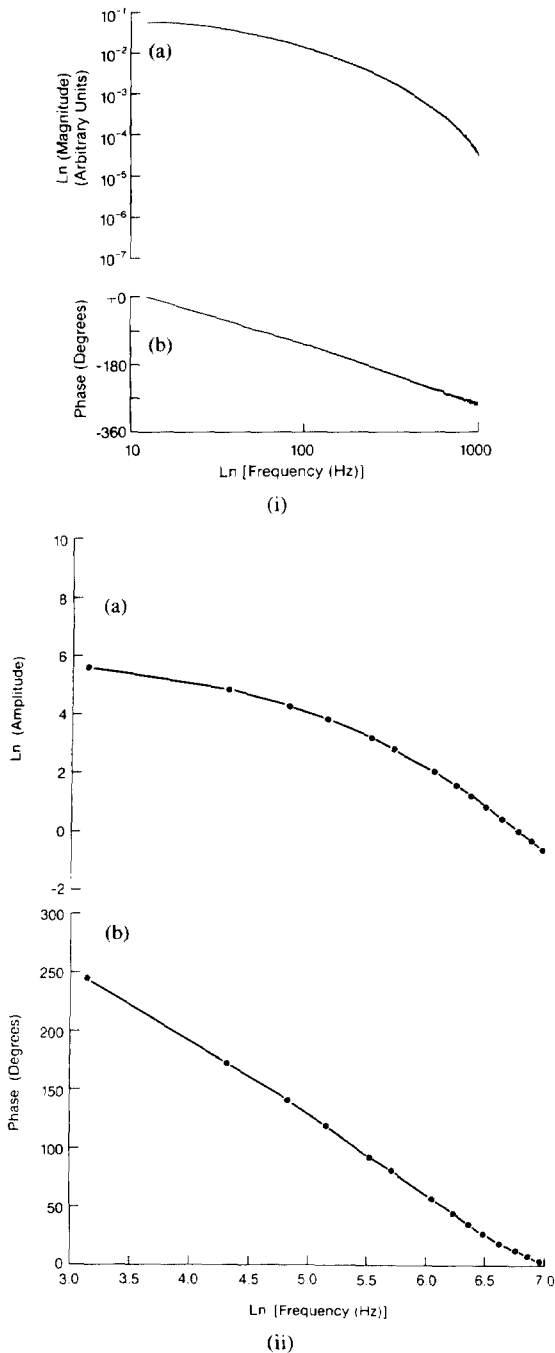


Fig. 33i). (a) Magnitude and (b) phase of the complex transfer function $H(f)$ of the blackbody/water interface at 10- μm probe beam offset, using the FM Time Delay Domain PDS apparatus. ii) (a) Amplitude and (b) phase of PDS signal with same data obtained using lock-in detection [11].

superior speed and reliability of the FM time-delay system make it a very attractive candidate for thermal mapping or depth-profiling applications in environments requiring fast turn-around, such as industrial quality control laboratories. Using a raised Hanning FIR filter (i.e., cosine to the fourth power window [14]), the input autocorrelation function $R_{xx}(\tau)$ was found to be extremely narrow on the time scale of the PDS experiments and could be accurately approximated by the Dirac delta function. According to (4.4), it follows that the input-output cross-

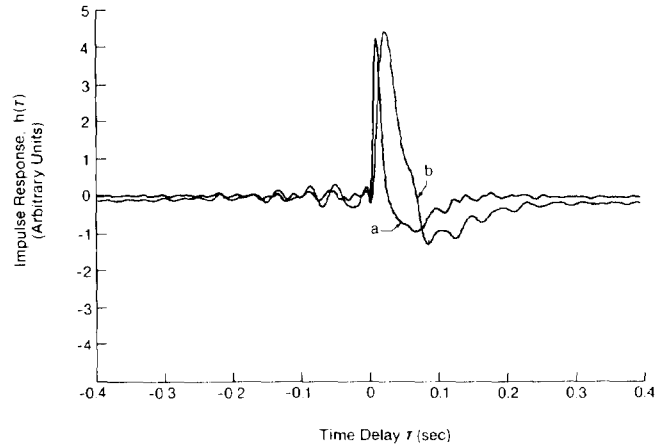


Fig. 34. Impulse response functions from quartz layers of thickness 30 μm (a), and 100 μm (b) [11].

correlation function is equal to the unit impulse response of the system; this was also verified experimentally [11].

The spectrometer was further used to measure the response from thin microscope quartz slide layers in direct contact with the backing material (anodized aluminum support). A single slide cut in many pieces was used for these experiments, to assure material uniformity. Each piece was etched in 50-percent HF : 50-percent H₂O down to the desired thickness. Fig. 34 shows a superposition of the impulse responses for two different thicknesses, 30 μm (Curve a) and 100 μm (Curve b). The cross-correlation functions show similar features, i.e., an increased peak delay time, a broadened FWHM, and an increased trough time delay τ_{min} with increasing thickness. In each case data were taken at beam offset positions that maximized the PDS output at the detector.

The secondary oscillations on both wings of the main pulse in Fig. 34 were found to be consistent with thermal energy arrivals at the sample surface after multiple reflections at the sample-backing interface. The delay time $\Delta\tau$ between two successive peaks corresponded roughly to twice the thermal transit time $\tau_{\text{transit}} = l^2/\alpha_2$ through the bulk of the sample. Similar effects have been predicted theoretically by Burt [62] in fluids excited by pulsed lasers and have been observed experimentally in liquids and solids by Tam *et al.* [9], [63].

A theoretical model for the impulse response of the PDS system was also presented by the authors of [11], who calculated the peak delay time τ_0 from the heat conduction Green's Function of the composite system:

$$\tau_0(l) = \frac{L_0^2}{6\alpha_3} [1 + (\alpha_3/\alpha_2)^{1/2} (l/L_0)]^2 \quad (5.1)$$

where α_1 , α_2 , and α_3 are the thermal diffusivities of the backing material, quartz layer, and water, respectively, and l and L_0 are the quartz layer thickness and probe beam offset at the beam-waist, respectively. A fit of (5.1) to the data gave a value of α_2 in good agreement with the published value [32]. Further experimentation with silicon wafer samples, on which 1- μm -thick field SiO₂ oxides

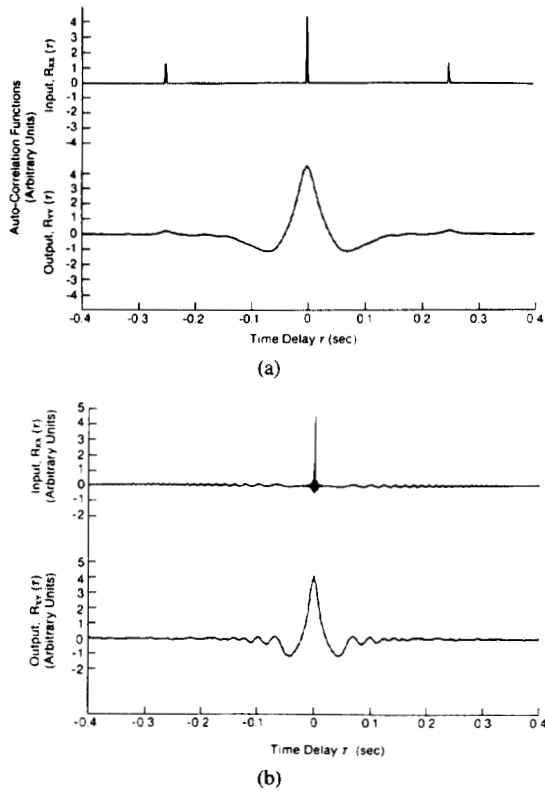


Fig. 35. Autocorrelation functions of system input and output. (a) FM time-delay method. (b) PRBS method ($N = 127$ bits) [12].

were grown thermally, showed that the FM time-delay-domain technique was quite sensitive to the presence of such oxides on the silicon surface [11]. These results were deemed promising for the future of the technique as a non-destructive semiconductor probe capable of replacing the pulsed laser excitation conventionally used [9], the two main advantages of the FM method being a) its much higher pulse tolerance threshold on sensitive materials such as those used in optoelectronic and microelectronic applications and b) its higher dynamic range than that of the impulsive excitation.

Mandelis *et al.* [12] further made a detailed comparison between FM time-delay and the PRBS methods of optical excitation and Mirage effect response. Fig. 35 shows a comparison of the autocorrelation functions $R_{xx}(\tau)$ and $R_{yy}(\tau)$ of inputs and outputs, respectively, of the two techniques. In Fig. 35(b) the secondary peaks of the PRBS input autocorrelation function are clearly seen at the onset of the second multiple of the frequency band spanned by the PRBS pseudo-period. These spikes are also present in the PRBS output autocorrelation, albeit much more broadened and of much lower magnitude. A comparison of $R_{xx}(\tau)$ between Figs. 35(a) and 35(b) shows that the PRBS function is more broadened than the FM time-delay function on the time scale of the experiment. Therefore, it is expected that the PRBS $R_{xx}(\tau)$ convolution with the impulse response (i.e., the input/output cross-correlation function, see (4.4)) will be somewhat broader than the PRBS impulse response function $h(\tau)$, a fact borne out by the experiments. On the other hand, the narrow $R_{xx}(\tau)$ of

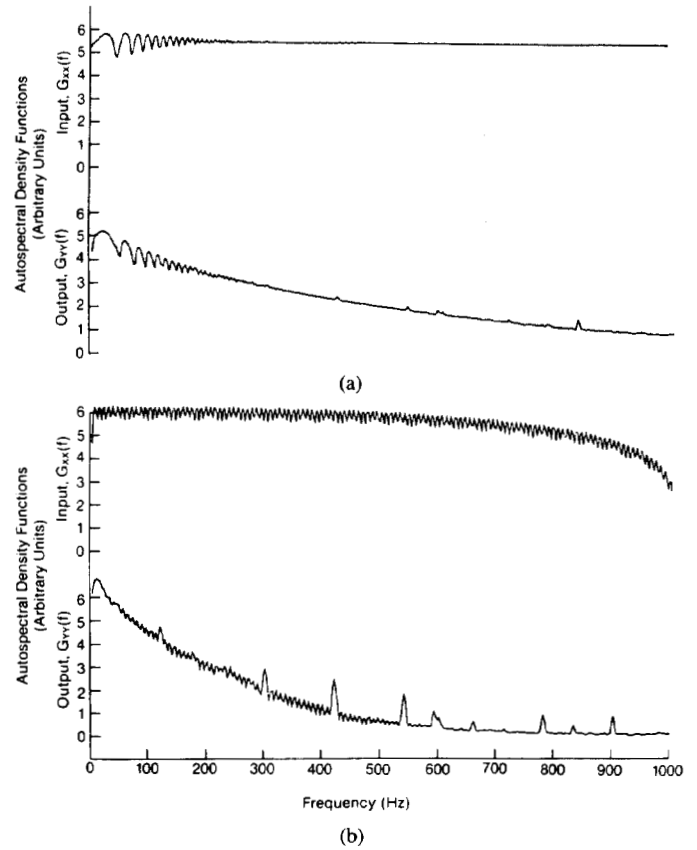


Fig. 36. One-sided autospectral densities of PDS system input and output. (a) FM time-delay method. (b) PRBS method [12].

the FM time-delay spectrometer is a closer representation of a Dirac delta function than the PRBS counterpart and produces essentially identical lineshapes between $h(\tau)$ and $R_{xx}(\tau)$.

Fig. 36 compares the one-sided autospectral densities of the two techniques between dc and 1 kHz. From this figure two facts become apparent immediately: First, the FM time-delay apparatus exhibits a truly flat input $G_{xx}(f)$ up to the highest frequency as expected from the Fourier transform of the Dirac delta function representing the autocorrelation of the input, and consistently with the condition (3.2'). The flat autospectral response of the FM technique guarantees the validity of the condition [64]

$$|(\Delta f)T| \gg 1 \quad (5.2)$$

with Δf given in (1.34). In practice, the physical requirement satisfied by the PDS system of [12] was

$$|\tau| \ll T \quad \text{for any } |\tau| \leq 1/|\Delta f| \quad (5.3)$$

i.e., the total sweep time was long compared to the time delay response of the system. This is a necessary condition for high delay time resolution of the technique. Second, Fig. 36(a) is to be compared to the decay of the PRBS spectral contributions of the average power above 200–300 Hz. The uneven distribution in the frequency density of the power input spectrum in the PRBS case results in a steeper decay of its output $G_{yy}(f)$ than the FM time-delay signal. This means that the higher frequency com-

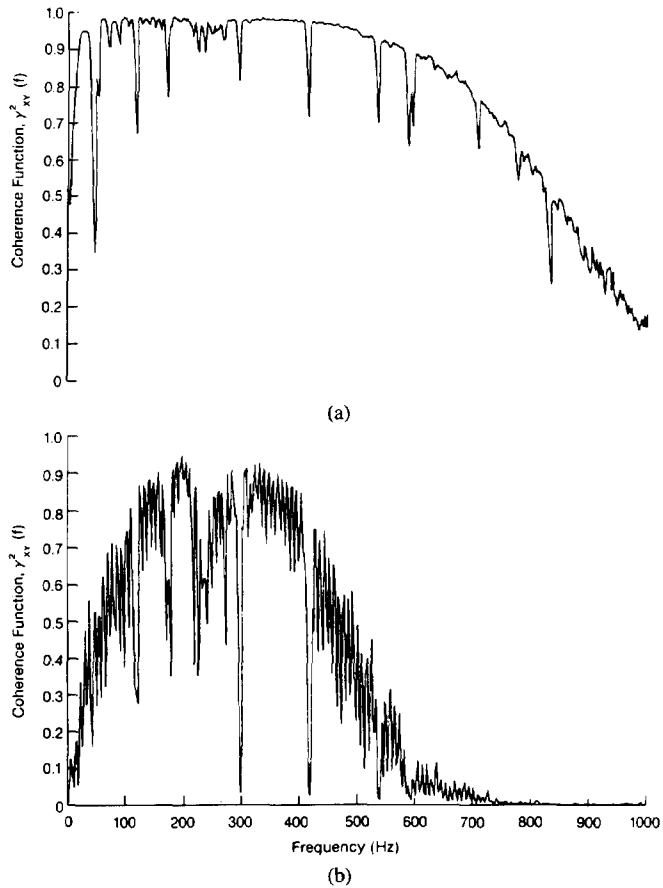


Fig. 37. Coherence function comparison. (a) FM time-delay method. (b) PRBS method [12].

ponents are weighed less in the PRBS experiment, with a concomitant spectral distortion at high frequencies. No indication of even the onset of such a frequency weighing phenomenon is shown by the FM time-delay spectrometer within the display frequency range. The flatness of the autospectral density function is a further assurance of the mathematical equivalence between the impulse response and cross-correlation functions (see (3.1)–(3.2')) for the FM time-delay spectrometer. Fig. 36(b) indicates that this equivalence is not entirely justified for the PRBS spectrometer, due to the autospectral density roll-off at high frequencies. It is further apparent from Fig. 36(b) that the autospectral density curve corresponding to PRBS excitation consists of discrete power bands ("saw-toothed" response) spanning narrow frequency ranges with a continuous envelope. The corresponding FM time-delay curve, on the other hand, is truly continuous aside from a progressively discrete behavior at frequencies below 200 Hz. The discrete power band regions in both Figs. 36(a) and 36(b) were seen to generate similar behavior of the output autospectral densities. This resulted in a saw-toothed output autospectral density $G_{yy}(f)$ for PRBS excitation, with a continuous envelope throughout much of the spectrum and was directly responsible for the lower quality of the PRBS signal.

Fig. 37 is a comparison between the coherence functions obtained from the signal inputs and outputs for the

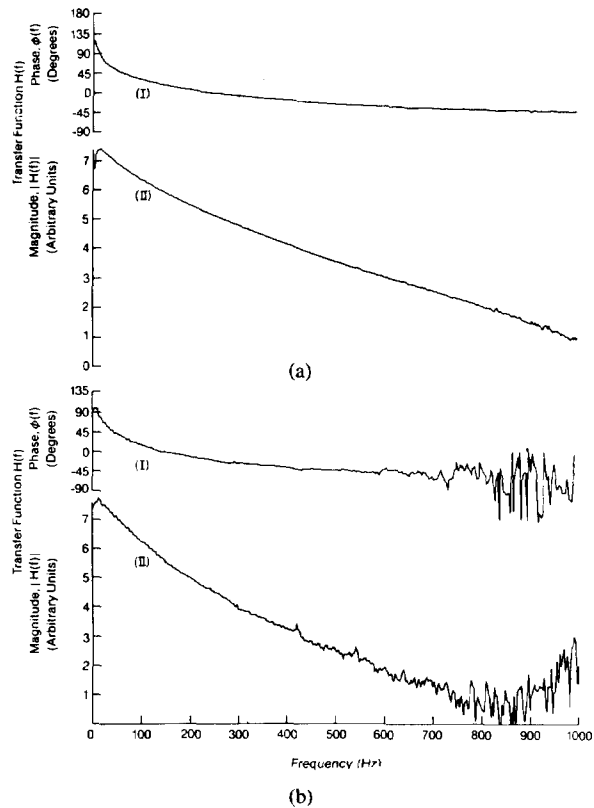


Fig. 38. Transfer function channels of the Mirage effect system. (a) FM time-delay method. (b) PRBS method. (I): Phase. (II) Magnitude [12].

two techniques. The coherence function is a most sensitive indicator of the quality of the relation between input and output. The superior performance of the FM time-delay spectrometer is unequivocally exemplified in this figure. Essentially no correlation can be found above 600 Hz for the PRBS method, while a strong relation between input and output well beyond 1 kHz is observed for the FM time-delay system. The dips in the coherence functions are due to non-system related deterministic signal sources, such as line ripple and multiples of 60 Hz. These sources are completely deterministic at well-defined frequencies and they do not appear in the statistics of the coherence function. The coherence of the PRBS system exhibited large discrete sawtoothed band components with peaks and valleys of rapidly varying functional quality of the relationship between input and output. This resulted in a poor signal-to-noise ratio of the transfer function $H(f)$, as seen in Fig. 38. This figure indicates the degree of dynamic range superiority of the FM time-delay spectrometer to that of the device operating with a PRBS excitation. The exceptional quality of the FM time-delay spectrometer transfer function is intimately related to the quality of the impulse response, whose Fourier transform the transfer function is.

VI. CONCLUSION

This review has shown that pseudorandom photothermal methods have become increasingly popular in recent years with investigators interested in depth-profiling,

```

C      PSEUDOSEQ.FTN
C      THIS PROGRAM GENERATES A PSEUDO-RANDOM SEQUENCE, 2**9-1=511 BITS IN
C      LENGTH.
C
C      INTEGER PSEUDO(513,9), I, J, ADD
C
C      PSEUDO(I,J) ULTIMATELY BECOMES THE 2-D ARRAY CONTAINING
C      THE M-SERIES PSEUDO-RANDOM BINARY SEQUENCE.
C      IN THIS CASE, THE SEQUENCE IS FOR 2**9=512 BITS, AND THE ARRAY
C      PARAMETERS REFLECT THIS.
C
C      I=1
C      DO 10 J=1,9
C          PSEUDO(I,J)=1
C      CONTINUE
C      DO 100 I=1,512
C
C          WRITE (2,15) PSEUDO(I,1),PSEUDO(I,2),PSEUDO(I,3),PSEUDO(I,4),
C          + PSEUDO(I,5),PSEUDO(I,6),PSEUDO(I,7),PSEUDO(I,8),PSEUDO(I,9)
C          FORMAT(1X,9I1)
C          ADD = PSEUDO(I,5) + PSEUDO(I,9)
C          DO 20 J=9,2,-1
C              PSEUDO(I+1,J) = PSEUDO(I,J-1)
C          CONTINUE
C          IF (ADD .EQ. 1) THEN
C              PSEUDO(I+1,1)=1
C          ELSE
C              PSEUDO(I+1,1)=0
C          END IF
C      CONTINUE
C      AMENDMENT TO TYPE OUT PRBS ITSELF....
C
C      K=1
C      DO 150 J=1,17
C          N=J*29
C          WRITE(2,17)(PSEUDO(I,9),I=K,N)
C          FORMAT(1X,29I2)
C          K=N+1
C          WRITE(2,16)(PSEUDO(I,9),I=K,511)
C          FORMAT(1X,18I2)
C      END

```

```

1 1 1 1 1 1 1 1 1 1 0 0 0 0 0 1 1 1 1 0 1 1 1 1 1 0 0 0 1 0
1 1 1 0 0 1 1 0 0 1 0 0 0 0 0 1 0 0 1 0 1 0 0 1 1 1 0 0 1 1
0 1 0 0 0 1 1 1 1 0 0 1 1 1 1 1 0 0 1 1 0 1 1 0 0 0 1 0 1
0 1 0 0 1 0 0 0 1 1 1 0 0 0 1 1 0 1 1 0 1 0 1 0 1 1 1 0 0
0 1 0 0 1 1 0 0 0 1 0 0 0 1 0 0 0 0 0 0 0 0 1 0 0 0 0 1 0
0 0 1 1 0 0 0 0 1 0 0 1 1 1 0 0 1 0 1 0 1 1 0 0 0 0 1
1 0 1 1 1 1 0 1 0 0 1 1 0 1 1 1 0 0 1 0 0 0 1 0 1 0 0 0 0
1 0 1 0 1 1 0 1 0 0 1 1 1 1 1 1 0 1 1 0 0 0 1 0 0 1 0 0 1 0
1 1 0 1 1 1 1 1 1 1 0 0 1 0 0 1 1 0 1 0 1 0 0 1 1 0 0 1 1 0
0 0 0 0 0 0 1 1 0 0 0 1 1 0 0 1 0 1 0 0 0 1 1 0 1 0 0 1 0
1 1 1 1 1 1 1 0 1 0 0 0 1 0 1 1 0 0 0 1 1 1 0 1 0 1 1 0 0
1 0 1 1 0 0 1 1 1 1 0 0 0 1 1 1 1 1 0 1 1 1 0 1 0 1 0 0 0 0
1 1 0 1 0 1 1 0 1 1 0 1 1 0 1 1 1 0 1 1 0 0 0 0 1 0 1 1 0 1 0
1 1 1 1 1 0 1 0 1 0 1 0 1 0 0 0 0 0 1 0 1 0 0 1 0 1 0 1 0 1
1 1 1 0 0 1 0 1 1 1 0 1 1 1 0 0 0 0 0 0 1 1 1 0 0 1 1 1 0
1 0 0 1 0 0 1 1 1 1 0 1 0 1 1 1 0 1 0 1 0 0 0 1 0 0 1 0 0
0 0 1 1 0 0 1 1 1 0 0 0 1 0 1 1 1 1 0 1 1 0 1 1 0 1 0 0 1 1
0 1 0 0 0 0 1 1 1 0 1 1 1 1 0 0 0 0

```

Fig. 39. Fortran listing of an m -series PRBS.

depth-resolution, and depth spectroscopic analysis. The main advantages of these techniques are their nondestructive character, speed of data acquisition, and information multiplexing which is much richer in content and more reliable than frequency domain photothermal methods. The mathematical impulse-response equivalent obtained by the pseudorandom methods has the advantage of a higher damage threshold and higher SNR than conventional time-domain pulsed-laser-induced photothermal signals. A very promising alternative to pseudorandom photothermal methods is the recently emerged FM time-delay-domain technique. The first reports by Mandelis *et al.* include a detailed examination of the FM time-delay and spectral dynamic functions of a PDS system, and comparison with PRBS excitation. The results demonstrated that the FM excitation technique is capable of producing superior quality time-delay and spectral function information when tested on a fast, flat transfer function PDS system. It thus appears that the FM time-delay pho-

toacoustic/photothermal wave technique and instrumentation holds excellent promise of favorably competing with the pseudorandom methods for nondestructive evaluation and depth-profiling applications in scientific research as well as in industrial development laboratories.

APPENDIX

A Fortran program listing for an m -series PRBS is given in Fig. 39.

REFERENCES

- [1] J. S. Bendat and A. G. Piersol, *Random Data: Analysis and Measurement Procedures*. New York: Wiley-Interscience, 1971, chap. 1.
- [2] D. A. McQuarrie, *Statistical Mechanics*. New York: Harper and Row, 1973, chap. 22.
- [3] R. B. Randall, "Frequency analysis," in *Brüel & Kjaer Technical Rev.*, 2nd ed. 1977, sect. 2.4.
- [4] J. S. Bendat, *Principles and Applications of Random Noise Theory*. New York: John Wiley, 1958, sect. 3.3
- [5] H. Coufal, "Fourier analysis of frequency domain multiplexed pho-

- toacoustic signals," *J. Photoacoust.*, vol. 1, no. 4, pp. 413-428, 1984.
- [6] A. Mandelis, "Frequency modulated (FM) time delay photoacoustic and Detection. Part I: Theoretical," *Rev. Sci. Instr.*, vol. 57, no. 4, pp. 617-621, 1986.
- [7] J. S. Bendat and A. G. Piersol, ch. 3, Table 3.3.
- [8] C. K. N. Patel and E. T. Nelson, "Opto-Acoustic spectroscopy of condensed matter," in *Lasers and Applications*, Berlin: Springer-Verlag, pp. 122-140, 1981.
- [9] H. Sontag and A. C. Tam, "Optical monitoring of photoacoustic pulse propagation in silicon wafers," *Appl. Phys. Lett.*, vol. 46, no. 8, pp. 725-727, 1985.
- [10] J. Trampe Broch, "On the Measurement of Frequency Response Functions," in *Brüel & Kjaer Technical Rev.*, no. 4, 1975.
- [11] A. Mandelis, L. M-L. Borm, and J. Tiessinga, "Frequency modulated (FM) time delay photoacoustic and photothermal wave spectroscopies. Technique, instrumentation and detection. Part II: Mirage Effect spectrometer design and performance," *Rev. Sci. Instr.*, vol. 57, no. 4, pp. 622-629, 1986.
- [12] —, "Frequency modulated (FM) time delay photoacoustic and photothermal wave spectroscopies. Technique, instrumentation and detection. Part III: Mirage effect spectrometer. Dynamic range and comparison to pseudorandom-binary-sequence (PRBS) method," *Rev. Sci. Instr.*, vol. 57, no. 4, pp. 630-635, 1986.
- [13] R. C. Heyser, "Acoustical measurements by time delay spectrometry," *J. Audio Eng. Soc.*, vol. 15, no. 4, pp. 370-382, 1967.
- [14] H. Biering and O.Z. Pedersen, "System Analysis and Time Delay Spectrometry (Part I)," *Brüel & Kjaer Technical Review*, No. 1, 1983.
- [15] J. R. Klauder, A. C. Price, S. Darlington, and W. J. Albersheim, "The theory and design of chirp radars," *Bell. Syst. Tech. J.*, vol. 39, no. 4, pp. 745-808, 1960.
- [16] D. R. Bromaghim and J. P. Perry, "A wideband linear FM ramp generator for long-range imaging radar," *IEEE Trans. Microwave Theory Tech.*, vol. MTT-26, no. 5, pp. 322-325, 1978.
- [17] A. Papoulis, "The Fourier Integral and its Applications," New York: McGraw-Hill, 1962.
- [18] R. C. Heyser, "Loudspeaker phase characteristics and time delay distortion: Part I," *J. Audio Eng. Soc.* vol. 17, no. 1, pp. 30-41, 1969.
- [19] —, "Concepts in the frequency and time domain response of loudspeakers," *Monitor-Proc. IREE*, pp. 67-76, Mar. 1976.
- [20] —, "Loudspeaker phase characteristics and time delay distortion: Part 2," *J. Audio Eng. Soc.*, vol. 17, no. 2, pp. 130-137, 1969.
- [21] E. Jahnke and F. Emde, *Tables of Functions*. New York: Dover, 1945, pp. 35-38.
- [22] S. Haykin, *Communication Systems*. New York: Wiley, 1978, chap. 4.
- [23] K. G. Beauchamp and C. K. Yuen, *Digital Methods for Signal Analysis*. London: George Allen & Unwin, 1979, chap. 5.
- [24] A. V. Oppenheim and R. W. Schaffer, *Digital Signal Processing*. Englewood Cliffs, NJ: Prentice-Hall, 1975, sect. 5.5
- [25] R. B. Blackman and J. W. Tukey, *The Measurement of Power Spectra*. New York: Dover, 1958.
- [26] S. W. Golomb, *Digital Communications with Space Applications* Englewood Cliffs, NJ: Prentice-Hall, 1964, pp. 40-41.
- [27] E. A. A. Sloan, "A comparison of linearly and quadratically modified spectral estimates of Gaussian signals," *IEEE Trans. Audio Electroacoust.*, vol. AU-15, pp. 56-65, 1967.
- [28] D. W. Hutchinson, "A new uniform pseudorandom number generator," *Commun. ACM*, vol. 9, pp. 432-433, 1966.
- [29] S. W. Golomb, *Shift Register Sequences*. San Francisco: Holden-Day, 1967.
- [30] Y. Sugitani, A. Uejima, and K. Kato, "Correlation photoacoustic spectroscopy," *J. Photoacoust.*, vol. 1, no. 2, pp. 217-236, 1982.
- [31] K. Kato, S. Ishino, and Y. Sugitani, "Correlation photoacoustics," *Chem. Lett. (Chem. Soc. Jpn)*, vol. 7, pp. 783-786, 1980.
- [32] A. Rosencwaig, *Photoacoustics and Photoacoustic Spectroscopy* (Chemical Analysis, vol. 57). New York: John Wiley, 1980.
- [33] K. R. Godfrey, "Correlation methods," *Automatica*, vol. 16, pp. 527-534, 1980.
- [34] G. F. Kirkbright, R. M. Miller, and A. Rzakiewicz, "Applications of cross-correlation signal recovery in Photoacoustics," *J. Phys. (Paris)*, vol. 44, no. 6, pp. C6-249-252, 1983.
- [35] H. Coufal, U. Möller, and S. Schneider, "Photoacoustic imaging using the Hadamard transform technique," *Appl. Opt.*, vol. 21, no. 1, pp. 116-120, 1982.
- [36] —, "Photoacoustic imaging using a Fourier transform technique," *Appl. Opt.*, vol. 21, no. 13, pp. 2339-2343, 1982.
- [37] H. Coufal and P. Hefferle, "Photothermal analysis of thin films," IBM Research Report RJ 4342 (47420), pp. 1-6, 1984.
- [38] D. E. Knuth, *The Art of Computer Programming: Vol. 2/Seminumerical Algorithms*, 2nd ed. Reading, MA: Addison-Wesley, 1981, chap. 3.2.
- [39] G. F. Kirkbright, R. M. Miller, and D. E. M. Spillane, "Depth resolved spectroscopic analysis of solid samples using photoacoustic spectroscopy," *Anal. Chem.*, vol. 56, no. 12, pp. 2043-2048, 1984.
- [40] A. Mandelis and B. S. H. Royce, "Time-domain photoacoustic spectroscopy of solids," *J. Appl. Phys.*, vol. 50, no. 6, pp. 4330-4338, 1979.
- [41] A. Uejima, D. Curtis, and Y. Sugitani, "Thermal diffusivity and contact resistance of solid materials as studied by correlation photoacoustics," *J. Photoacoust.*, vol. 1, no. 4, pp. 397-411, 1984.
- [42] Y. Sugitani and A. Uejima, "Effect of M-series PRBS Modulation on the time resolution in correlation photoacoustics," *Bull. Chem. Soc. Jpn.*, vol. 57, pp. 2023-2024, 1984.
- [43] A. Mandelis and J. T. Dodgson, "Spectroscopic studies of solids via correlation photoacoustic spectroscopy (CPAS)," *J. Phys. C: Solid State Phys.*, to be published.
- [44] J. T. Dodgson, A. Mandelis, and C. Andretta, "Optical absorption coefficient measurements in solids and liquids using correlation photoacoustic spectroscopy," *Can. J. Phys.*, to be published.
- [45] G. F. Kirkbright and R. M. Miller, "Cross-correlation techniques for signal recovery in thermal wave imaging," *Anal. Chem.*, vol. 55, no. 3, pp. 502-506, 1983.
- [46] H. Coufal, "Photothermal spectroscopy using a pyroelectric thin-film detector," *Appl. Phys. Lett.*, vol. 44, no. 1, pp. 59-61, 1984.
- [47] A. Mandelis, "Frequency-domain photopyroelectric spectroscopy of condensed phases (PPES): A new, simple and powerful spectroscopic technique," *Chem. Phys. Lett.*, vol. 108, no. 4, pp. 388-392, 1984.
- [48] A. Rosencwaig and A. Gersho, "Theory of the photoacoustic effect with solids," *J. Appl. Phys.*, vol. 47, no. 1, pp. 64-69, 1976.
- [49] A. Mandelis, Y. C. Teng, and B. S. H. Royce, "Phase measurements in the frequency domain photoacoustic spectroscopy of solids," *J. Appl. Phys.*, vol. 50, no. 11, pp. 7138-7146, 1979.
- [50] Y. Sugitani and A. Uejima, "Depth resolved thermal wave imaging of layer-structured sample by correlation photoacoustics," *Chem. Lett. (Chem. Soc. Jpn)*, vol. 12, pp. 397-400, 1985.
- [51] R. M. Miller "Digital simulation of photoacoustic impulse responses," *Can. J. Phys.*, to be published.
- [52] J. Crank, *The Mathematics of Diffusion*. Oxford: Clarendon 1975.
- [53] A. Mandelis and B. S. H. Royce, "Nonradiative lifetime measurements in time-domain photoacoustic spectroscopy of condensed phases," *J. Appl. Phys.*, vol. 51, no. 1, pp. 610-615, 1980.
- [54] G. K. Kirkbright, R. M. Miller, D. E. M. Spillane and I. P. Vickery "Impulse response photoacoustic spectroscopy of biological samples," *Analyst*, vol. 109, pp. 1443-1447, 1984.
- [55] A. Uejima, Y. Sugitani, and K. Nagashima, "Depth resolved spectroscopic analysis of color reversal films by correlation photoacoustics," *Anal. Sci.*, vol. 1, pp. 5-8, 1985.
- [56] R. M. Miller, G. R. Surtees, C. T. Tye, and I. P. Vickery "The study of time-dependent phenomena in materials by impulse response Photoacoustic Spectroscopy," *Can. J. Phys.*, to be published.
- [57] M. J. Adams and G. F. Kirkbright "Thermal diffusivity and thickness measurements of powdered solid samples utilizing the photoacoustic effect," *Analyst*, vol. 102, pp. 678-682, 1977.
- [58] K. D. Carlson and D. Hodul "Dilution effects in the photoacoustic spectra of powdered H_2O_3 and Er_2O_3 mixtures," *J. Photoacoust.*, vol. 1, no. 2, pp. 291-307, 1982.
- [59] J. C. Roark, R. A. Palmer, and J. S. Hutchison "Quantitative absorption spectra via photoacoustic phase angle spectroscopy (ϕ AS)," *Chem. Phys. Lett.*, vol. 60, no. 1, pp. 112-116, 1978.
- [60] M. F. Cox and G. N. Coleman, "Measurement of single-pulse photoacoustic signals," *Anal. Chem.*, vol. 53, no. 13, pp. 2034-2036, 1981.
- [61] W. B. Jackson, N. M. Amer, A. C. Boccara, and D. Fournier, "Photothermal deflection spectroscopy and detection," *Appl. Opt.*, vol. 20, no. 8, pp. 1333-1344, 1981.
- [62] J. A. Burt "Extension of the theory of the fluid-filled photoacoustic cell," *J. Phys. D: Appl. Phys.*, vol. 13, pp. 1985-1995, 1980.
- [63] A. C. Tam and C. K. N. Patel "Optical absorptions of light and heavy water by laser photoacoustic spectroscopy," *Appl. Opt.*, vol. 18, no. 19, pp. 3348-3358, 1979.
- [64] H. Biering and O. Z. Pedersen, "System Analysis and Time Delay Spectrometry (Part II)," *Brüel & Kjaer Technical Review*, no. 2, 1983.



Andreas Mandelis was born in Corfu (Kerkira), Greece on June 22, 1952. He received the B.S. degree in physics from Yale University, New Haven, CT, and the M.A. degree in applied physics, the M.S.E. degree in mechanical and aerospace engineering, and the Ph.D. degree in applied physics from Princeton University, Princeton, NJ.

From 1979 to 1981 he was a Member of the Scientific Staff with Bell Northern Research, Ottawa, Canada, involved in silicon research and

development. Since 1981 he has been Assistant Professor with the Department of Mechanical Engineering, University of Toronto, ON, Canada.

Dr. Mandelis is a member of the American Physical Society, Sigma Xi, the Canadian Association of Physicists, the Spectroscopy Society of Canada, and the New York Academy of Sciences.
